Journal of Materials Chemistry A

ROYAL SOCIETY OF CHEMISTRY

REVIEW

View Article Online
View Journal | View Issue

Cite this: J. Mater. Chem. A, 2022, 10, 8087

Recent advances in various applications of nickel cobalt sulfide-based materials

Gaofei Xue,[ab] Tian Bai,[ab] Weiguo Wang,[ab] Senjing Wang[b] and Meidan Ye *[ab]

Received 13th January 2022
Accepted 7th March 2022

DOI: 10.1039/d2ta00305h

rsc.li/materials-a

In recent years, nickel cobalt sulfides (NCSs) have received much attention as promising functional materials in various application fields, mainly due to their much lower price, abundant raw materials and considerable reactive activity with relatively higher electrical conductivity, weaker metal–sulfur bonds and better thermal stability compared to their oxide counterparts. In this review, we will briefly summarize the recent development of NCSs on the aspects of structural design, component optimization and composite preparation. Moreover, we will comprehensively review the recent applications of NCS nanomaterials in various fields (*e.g.*, supercapacitors, batteries, electrocatalysis, photocatalysis, sensors and microwave absorption), and some representative examples will be highlighted for different applications of NCSs. Finally, we will outline the common problems and prospects of NCS nanomaterials used in various applications.

1. Introduction

In recent years, transition metal chalcogenides have caught much research attention owing to their unique physicochemical characteristics, low cost, and broad application potential.[1–7] Among them, ternary sulfides have drawn rather extensive interest in the field of energy conversion and storage (*e.g.*, solar cells, water splitting, hydrogen generation, supercapacitors, Li/Na-ion (Li–S, Li–O_2, and Zn–air) batteries, *etc.*) because of their outstanding electrochemical performance.[8,9] In particular, nickel cobalt sulfides (NCSs) have become one of the most concerned ternary sulfides, mainly due to their relatively high electrical conductivity, multiple valence states and rich crystallographic structures.[10,11] It is generally considered that nickel holds tetrahedral sites, while cobalt takes over both octahedral and tetrahedral sites within spinel $NiCo_2S_4$ (Fig. 1). The mixture of heterogeneous spin states from Ni and Co atoms will result in lattice distortion and subtle atomic arrangement due to the mismatch in the Jahn–Teller distortion degree (Co^{2+}, $t2g^6eg^1$, strong John–Teller effect; Ni^{2+}, $t2g^6eg^2$, no John–Teller effect), which would produce more exposed active octahedral edge sites of NCSs.[12] This is beneficial for more electrochemical reactions (*e.g.*, pseudocapacitor or catalysis) and thus the synergistic effect between Ni and Co can effectively boost the electrochemical performance of NCSs with the coexistence of Ni^{2+}, Ni^{3+}, Co^{2+}, and Co^{3+} ions. Compared to nickel cobalt oxides (Fig. 1), NCSs present relatively lower optical energy band gaps

[a]Shenzhen Research Institute of Xiamen University, Shenzhen 518057, China. E-mail: mdye@xmu.edu.cn

[b]Research Institute for Biomimetics and Soft Matter, Fujian Provincial Key Laboratory for Soft Functional Materials Research, Department of Physics, Xiamen University, Xiamen 361005, China

Gaofei Xue received his B.S. in Material Physics from Fujian Normal University, China in 2020. He is now a graduate student in the College of Physical Science and Technology, Xiamen University, China. He joined Professor Meidan Ye's group in 2020. His research focuses on flexible materials and devices.

Tian Bai received his B.S. from the Shaanxi University of Science & Technology, China in 2018. He is now a graduate student in the College of Physical Science and Technology, Xiamen University, China. He joined Professor Meidan Ye's group in 2019. His research focuses on 2D material-based flexible devices.

($NiCo_2S_4$: 1.2 eV *vs.* $NiCo_2O_4$: 2.5 eV) and higher conductivity (~100 times).[13,14] This enables the lowering of the charge-transfer resistance of NCSs and facilitates charge transport when they are applied in energy conversion and storage systems. Theoretical calculation results indicate that $NiCo_2S_4$ has a smaller band gap than $NiCo_2O_4$ (Fig. 1d and e), suggesting its higher electric conductivity. And $NiCo_2S_4$ possesses a lower diffusion energy than $NiCo_2O_4$ (Fig. 1c), revealing that ions can more easily diffused in $NiCo_2S_4$.[15] The replacement of oxygen by sulfur for NCSs will create more flexible structures since the electronegativity of sulfur is lower than that of oxygen.[16] This can alleviate the structural deformation originating from the intercalation of electrolyte ions and thus promote the reactions between electrolyte ions and NCSs, yielding much enhanced electrochemical performance.

In recent years, much effort has been devoted to the development of NCSs, which can be roughly divided into several aspects.

The first is the design of micro-/nano-structures (Fig. 2 and 3). In addition to conventional nanostructures (*e.g.*, zero-dimensional (0D) nanoparticles,[17] one-dimensional (1D) nanowires/nanorods/nanotubes,[18,19] and two-dimensional (2D) nanosheets[20]), some special morphologies as well have been designed, such as nanotube-woven hexagonal microsheets,[21] nanosheet-constructed hollow nanocages,[22] nanoparticle-stacked microspheres,[23] hexagonal nanoplate-assembled microstructures,[24] and so on. Such hierarchical structures are beneficial to further amplify the active reaction sites, facilitate the charge transport and promote the ion diffusion, ultimately strengthening the performance of NCSs.[25–28] Although the hydrothermal/solvothermal method is still the most common way to synthesize the nanostructures of NCS materials,[29] multi-step strategies combining different processes (*e.g.*, solution reactions (hydrothermal/solvothermal, sol–gel and chemical bath reactions), electrodeposition and high-temperature calcination) are becoming more and more popular to construct high-performance morphologies of NCSs.[30,31] More impressively, *in situ* growth of NCS nanostructured films directly onto conductive substrates (*e.g.*, carbon cloth and Ni foam; Fig. 2 and 3d–f) is also well accepted mainly because it enables the simplification of the synthesis processes, removal of the use of binders, avoidance of the aggregation of nanomaterials, and reduction of the interfacial resistance between NCS films and substrates, therefore improving the performance of NCSs.[19,32]

The second is the study of the stoichiometric effect. For ternary or quaternary semiconductors, the stoichiometric ratio of their elements is usually adjustable, which also plays an important role in their properties and device performance.[33,34] A variety of studies have been performed to investigate this stoichiometric effect on NCSs, and various NCSs with different element stoichiometry have been prepared, such as $NiCo_2S_4$,[19,35] $CoNi_2S_4$,[36,37] $Ni_{1.4}Co_{1.6}S_4$,[38] $Ni_{1.5}Co_{1.5}S_4$,[39] $(Co_{0.5}Ni_{0.5})_9S_8$,[40] $(Ni_{0.33}Co_{0.67})_9S_8$,[41] $Ni_{1.77}Co_{1.23}S_4$,[42] $Ni_{4.5}Co_{4.5}S_8$,[43] $Ni_{0.67}Co_{0.33}S$,[44] *etc.* The comparison of the relative performance of NCSs with different element stoichiometry has also been discussed in depth (Fig. 4).[45] It is proposed that the high conductivity of NCSs is mainly due to the occupation of Ni in the tetrahedral sites of the spinel structure, the low bandgap and the synergistic coupling effect between Co and Ni with p-type (Co) and n-type (Ni) doping.[46] Then, the different ratios of Ni/Co contents in NCSs will influence their performance in applications. For example, three NCSs with varied Ni/Co ratios ($Ni_{0.8}Co_{2.2}S_4$, $Ni_{1.5}Co_{1.5}S_4$, and $Ni_{2.2}Co_{0.8}S_4$) were synthesized to study the

Weiguo Wang received his B.S. from Fujian Agriculture and Forestry University, China in 2019. He is now a graduate student in the College of Physical Science and Technology, Xiamen University, China. He joined Professor Meidan Ye's group in 2019. His research focuses on flexible materials and devices.

Senjing Wang received his B.S. in Measurement Control Technology and Instruments from Xiamen University, China in 2021. He is now a graduate student in the College of Physical Science and Technology, Xiamen University, China. He joined Professor Meidan Ye's group in 2021. His research focuses on energy storage materials and devices.

Meidan Ye received her PhD from the College of Chemistry and Chemical Engineering at Xiamen University in 2014. She then joined the Research Institute for Soft Matter and Biomimetics, Department of Physics, College of Physical Science and Technology at Xiamen University as an associate Professor in 2014. She was promoted to a Professor in 2021. Her research interests are on multifunctional materials for flexible devices, i.e., electrochemical energy storage devices and wearable sensors.

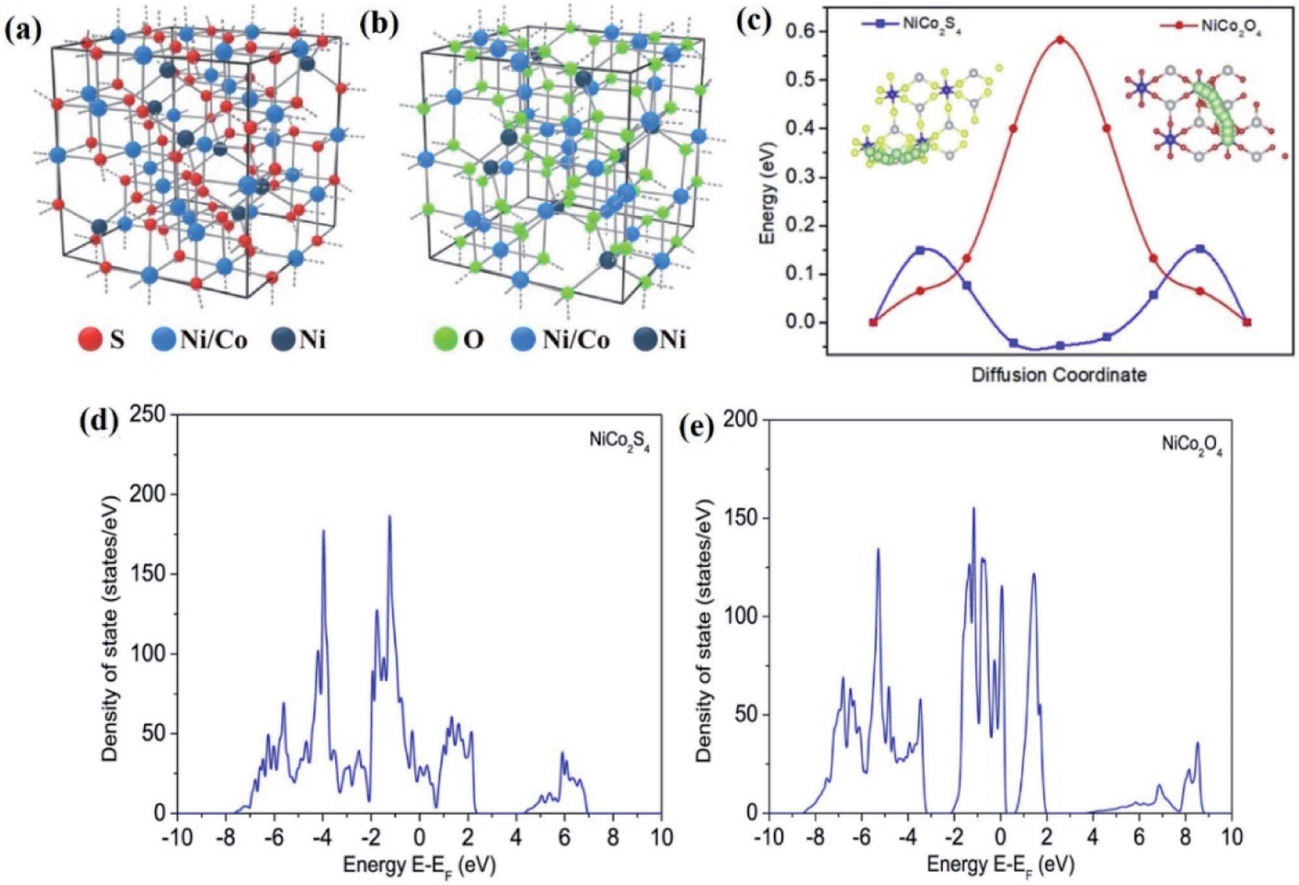

Fig. 1 Schematic diagram of the crystal structures of (a) $NiCo_2S_4$ and (b) $NiCo_2O_4$. (c) The Li ion diffusion battier energies and (d and e) the density of states (DOS) of $NiCo_2S_4$ and $NiCo_2O_4$ calculated by using density functional theory (DFT) simulation.[15] Reproduced from ref. 10 with permission from Elsevier.

composition effect on their electrocatalytic activity.[47] It was found that $Ni_{2.2}Co_{0.8}S_4$ had the highest current density and the lowest overpotential for the oxygen evolution reaction (OER) due to its largest content of Ni^{3+} with the conversion of Ni^{3+} to Ni^{4+} for producing more active sites to adsorb –OOH, while $Ni_{1.5}Co_{1.5}S_4$ exhibited the highest current density for the oxygen reduction reaction (ORR) owing to the larger content of Ni^{2+} and Co^{2+} with superior conductivity and the synergetic coupling between Ni and Co.[47]

The third is the fabrication of composites. NCS-based composites also have been widely fabricated to compensate for the shortcomings of NCSs (*e.g.*, relatively low stability and slow mass transfer/reaction kinetics). NCSs can be rationally integrated with lots of other materials, for example, metal oxides (*e.g.*, CeO_2,[54] $CoMoO_4$,[55] $NiCo_2O_4$,[43] Co_3O_4,[56] *etc.*), sulfides (*e.g.*, $FeCo_2S_4$,[57] Co_9S_8,[58] MgS,[59] MoS_2,[60] SnS_2,[61] *etc.*), selenides (*e.g.*, $Co_{0.85}Se$,[62] $MoSe_2$,[63] *etc.*), phosphides (*e.g.*, NiCoP,[64] NiFeP,[65] *etc.*), carbon-based materials (*e.g.*, carbon nanotubes (CNTs),[66] graphene,[67–69] carbon dots,[70] mesoporous carbon spheres,[71] *etc.*), polymers (*e.g.*, polypyrrole,[72] polyanilnie,[73] *etc.*), layered double hydroxides (LDHs; NiMn-LDHs,[74] CoNo-LDHs,[75] NiFe-LDHs,[76] *etc.*), two-dimensional titanium carbide (MXene),[77] and others (*e.g.*, g-C_3N_4,[78] Ag,[44] *etc.*). Besides, element doping (*e.g.*, Mn,[79] and Cu[80]) also have been widely used to further enhance the performance of NCSs.

The fourth is the development of applications (Fig. 2). NCSs are one type of the most popular electrode material used in supercapacitors due to their excellent electrochemical activity.[53,81] Besides, NCSs have been gradually applied to other electrochemical energy storage systems over the years, mainly including Li/Na-ion batteries,[18,82] Li–O_2 batteries,[83] Zn–air batteries,[69] and Li–S batteries.[35] NCSs are also able to act as effective counter electrodes in dye/quantum dot-sensitized solar cells (DSCs/QDSCs).[84,85] NCSs as well have great activity in photocatalytic reactions, such as the degradation of organic pollution and hydrogen evolution.[86,87] Moreover, NCSs can be efficient electrocatalysts for overall water splitting with bi-functions of the oxygen evolution reaction (OER) and hydrogen evolution reaction (HER).[88,89] Particularly, NCSs can be used as bio-sensing materials due to their attractive electrochemical characteristics[90] and microwave absorbers because of their excellent magnetic loss properties.[91]

For NCSs, some articles have reviewed their applications in supercapacitors and batteries.[1,10,11] However, few reviews comprehensively summarize promising applications for NCSs in different fields. In this review, we focus on the recent

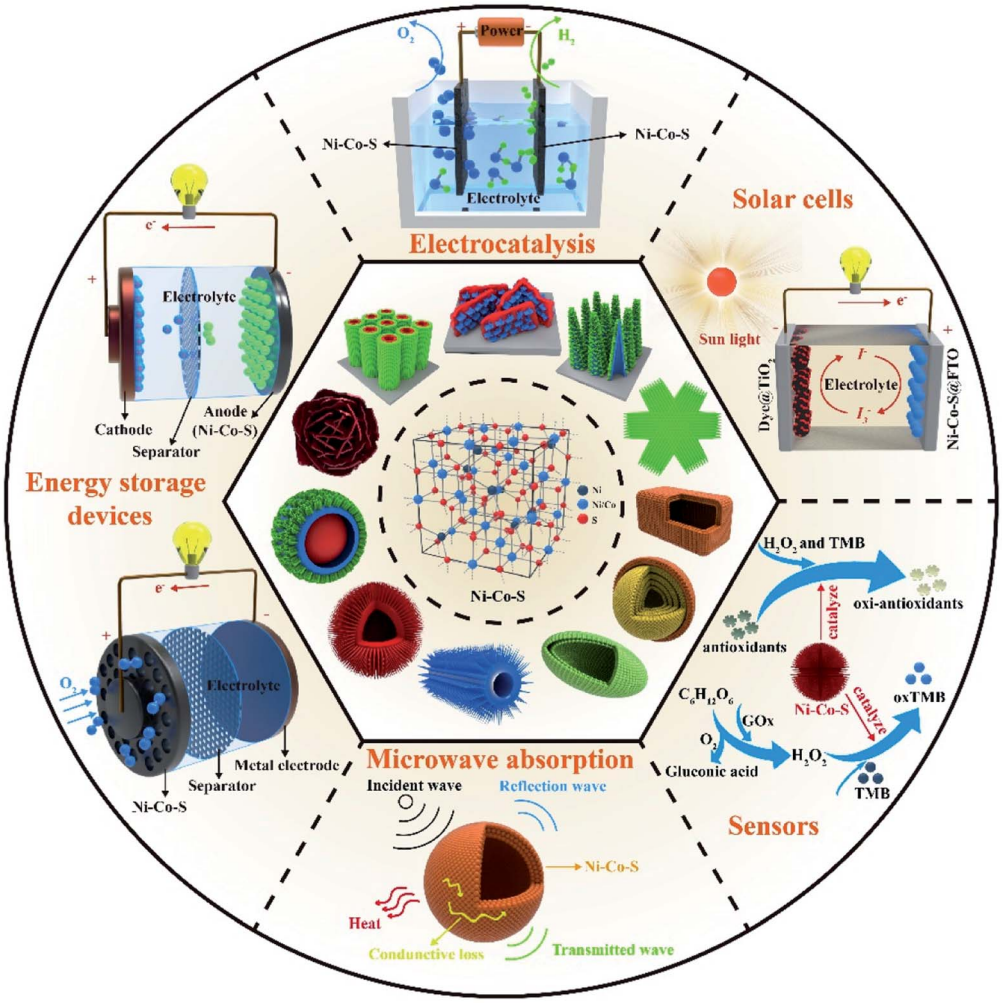

Fig. 2 Schematic diagrams of the crystal structures, nanostructures and applications of NCSs.

applications of NSCs in a variety of fields in the last few years. We discuss some representative studies about the applications of NCSs in energy storage devices, electrocatalysis, photocatalysis, sensors and microwave absorption. We highlight the intercommunity of NCSs in different application fields. Finally, the general problems and future prospects of NCSs for various applications are analyzed and emphasized.

2. Applications of NCSs in energy storage devices

2.1. Supercapacitors

NCSs have been intensively applied in supercapacitors due to their relatively higher conductivity and more redox sites in comparison with their corresponding oxides and binary sulfides. It is commonly considered that the pseudocapacitive performance of NCSs is mainly due to the Faraday redox reactions between Ni^{2+}/Ni^{3+} and Co^{2+}/Co^{3+}. In an alkaline aqueous electrolyte, the reversible Faraday peaks can be associated with the reversible redox reactions from $NiCo_2S_4$ to NiSOH, CoSOH and CoSO species (Fig. 5). The theoretical capacitance of $NiCo_2S_4$ in supercapacitors is 2534 F g^{-1}.[1]

In order to amplify the charge storage ability of NCSs, a series of strategies have been developed (Table 1), including regulating the element ratio (*e.g.*, $NiCo_2S_4$,[19,35] $CoNi_2S_4$ [36,37] and $NiCo_2S_{4-x}$ [19]), tuning the morphological structures in different dimensions (Fig. 6a and b),[45,92–94] doping other elements (*e.g.*, Fe,[95] Mn,[96] P,[29] and V;[97] Fig. 6d–f), and integrating with other materials (*e.g.*, CNTs,[98] graphene,[63] Nb_2O_5,[99] $Ni(OH)_2$,[100] $FeCo_2S_4$,[57] MXenes,[77] *etc.*). For example, the defect engineering strategy enables the production of rich sulfur vacancies on the surface of NCS crystals through various methods, such as low-temperature plasma induction (Fig. 4h–j),[20] Ar/H_2 gas-assisted annealing,[23] and $NaBH_4$ solution reduction.[30] The existence of sulfur vacancies will change the electronic structures of NCSs to increase their conductivity and reactive sites for enhanced electrochemical performance.[20] Besides, the 3D hierarchical structures of NCSs (Fig. 6) have been widely designed and fabricated for high-performance supercapacitors,[93,101–103] mainly because they have attractive properties to offer sufficient surface

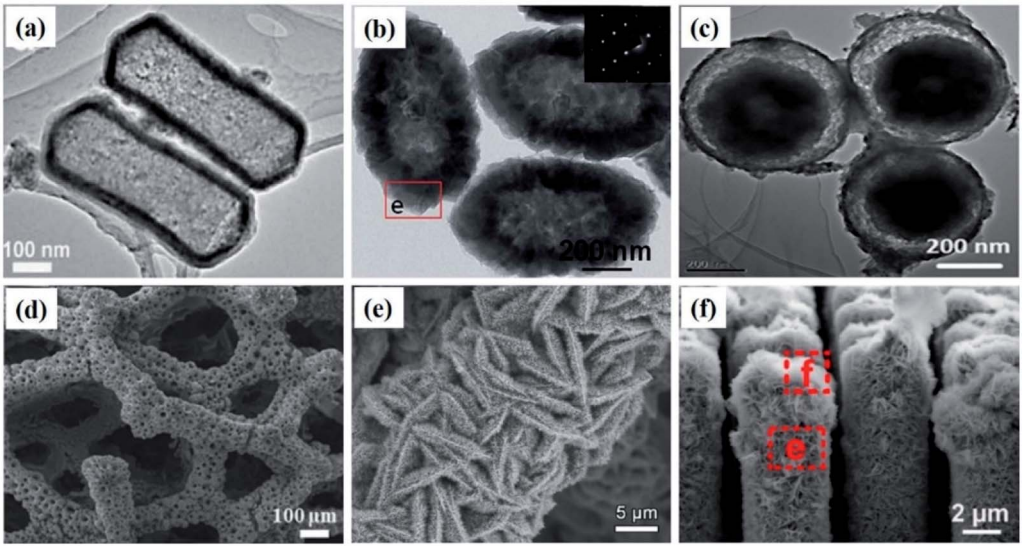

Fig. 3 Some representative NCS structures: transmission electron microscopy (TEM) images of (a) $NiCo_2S_4$ @ N-doped carbon hollow capsules,[48] (b) $NiCo_2S_4/Co_9S_8$ submicro-spindles,[49] and (c) $NiCo_2S_4$ double-shelled ball-in-ball hollow spheres;[50] SEM images of (d) $NiCo_2S_4$ nanosheets @ Ni foam,[51] (e) caterpillar-like $NiCo_2S_4$ arrays @ carbon cloth,[52] and (f) $NiCo_2S_4$ nanosheets @ Ni columns.[53] Reproduced from ref. 17, 18, 20 and 21 with permission from the Royal Society of Chemistry. Reproduced from ref. 19 and 22 with permission from American Chemical Society.

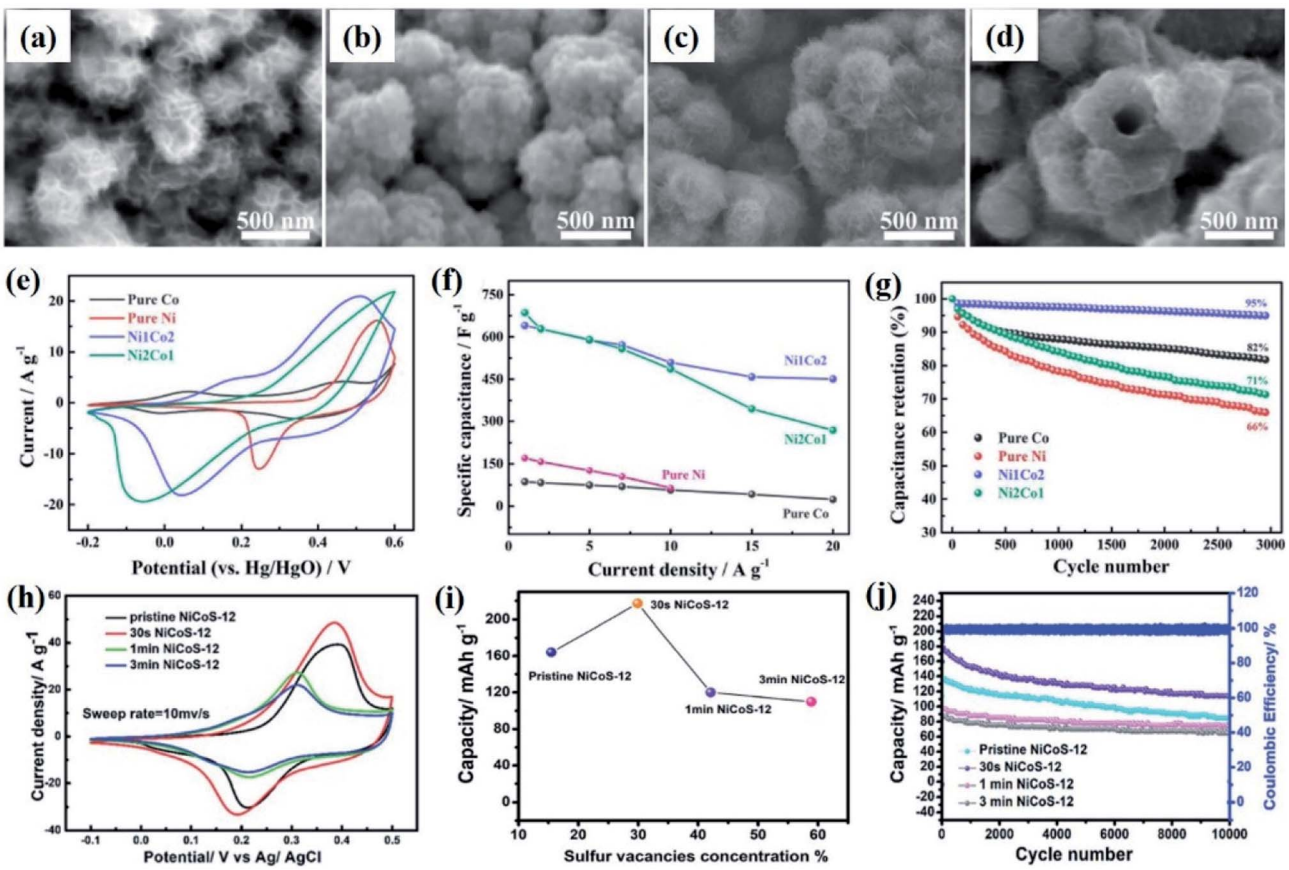

Fig. 4 SEM images (a–d) and electrochemical performance (e–g) of metal sulfides composed of different Ni/Co molar ratios: (a) pure Co, (b) pure Ni, (c) 1/2, and (d) 2/1.[45] Electrochemical performance (h–j) of $NiCo_2S_4$ films with different concentrations of surface sulfur vacancies.[20] Reproduced from ref. 60 with permission from American Chemical Society. Reproduced from ref. 61 with permission from the Royal Society of Chemistry.

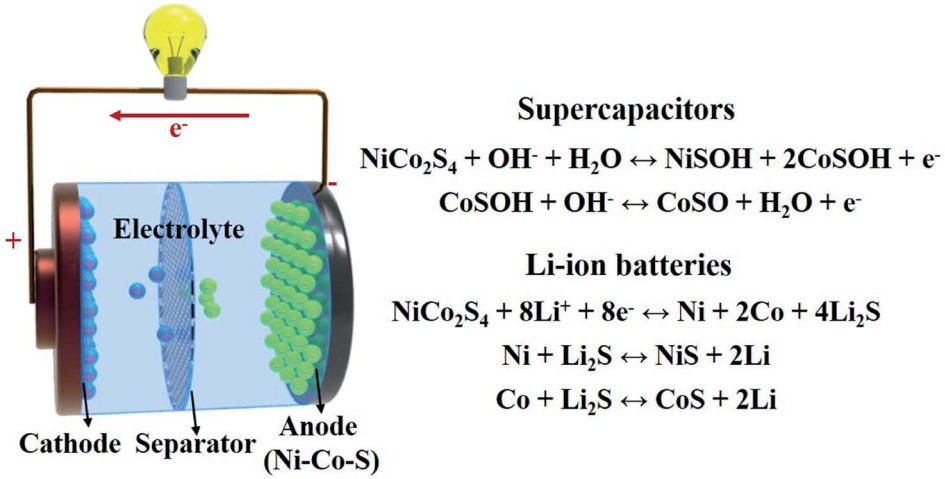

Fig. 5 Schematic diagram and reactions of NCSs in supercapacitors and Li-ion batteries.

areas for more faradaic redox reactions, and build fast channels for effective charge transfer and ion diffusion.

It is worth noting that NCSs frequently show obvious battery-like charge storage behavior, that is, displaying typical redox peaks in cyclic voltammogram curves (CVs; *vs.* near-rectangular shapes or broadened peaks for capacitors; Fig. 6c) and clear discharge platforms in galvanostatic charge/discharge curves (GCDs; *vs.* quasi-triangular shapes for capacitors; Fig. 6e).[105] It means that the reaction kinetics of NCSs in the charge storage processes are partially determined by the diffusion-controlled redox behavior (*i.e.*, $I \propto v^{\frac{1}{2}}$, where I is the current and v is the scan rate in CVs), while the reaction kinetics of pseudocapacitance are dominated by the surface-controlled faradaic process (*i.e.*, $I \propto v$).[58] Thus, the corresponding devices based on battery-like NCS electrodes are named hybrid supercapacitors due to the capacity contribution both from the diffusion-controlled

Table 1 Performance of different NCS-based materials in supercapacitors

Material	Capacitance/capacity of electrodes	Capacitance/capacity of devices	Energy density/power density of devices	Cycling stability of devices	Ref.
$Ni_3S_2/CoNi_2S_4$ porous network	2435 F g^{-1} @ 2 A g^{-1}	175 F g^{-1} @ 1 A g^{-1}	40.0 W h kg^{-1}/17.3 kW kg^{-1}	92.8% capacitance retention after 6000 cycles @ 10 A g^{-1}	111
$ZnS/NiCo_2S_4/Co_9S_8$ nanotubes	1618.1 F g^{-1} @ 1 A g^{-1}	—	66 W h kg^{-1}/0.75 kW kg^{-1}	62% capacitance retention after 5000 cycles @ 5 A g^{-1}	112
Ni–Co–S nanosheets @ graphene foam	2918.1 F g^{-1} @ 1 A g^{-1}	209.82 F g^{-1} @ 1 A g^{-1}	79.3 W h kg^{-1}/0.83 kW kg^{-1}	54.02% capacitance retention after 10 000 cycles @ 5 A g^{-1}	113
Zn-doped Ni–Co–S nanocomposite	2668 F g^{-1} @ 1 A g^{-1}	150 F g^{-1} @ 1 A g^{-1}	60.2 W h kg^{-1}/0.85 kW kg^{-1}	91.2% capacitance retention after 10 000 cycles @ 5 A g^{-1}	114
$NiCo_2S_4$/MXene	1028C g^{-1} @ 1 A g^{-1}	171.2 F g^{-1} @ 1 A g^{-1}	68.7 W h kg^{-1}/0.85 kW kg^{-1}	89.5% capacitance retention after 5000 cycles @ 5 A g^{-1}	77
NiFeP@$NiCo_2S_4$ nanosheets	874.4C g^{-1} @ 1 A g^{-1}	197.6 F g^{-1} @ 1 A g^{-1}	87.9 W h kg^{-1}/0.43 kW kg^{-1}	85.2% capacitance retention after 10 000 cycles @ 8 A g^{-1}	65
$MoS_2/NiCo_2S_4$@C hollow microspheres	250 mA h g^{-1} @ 2 A g^{-1}	120 F g^{-1} @ 1 A g^{-1}	53.01 W h kg^{-1}/4.20 kW kg^{-1}	90.1% capacitance retention after 10 000 cycles @ 10 A g^{-1}	115
Carbon nanofiber/ $NiCo_2S_4$ nanosheets @ polypyrrole	2961 F g^{-1} @ 1 A g^{-1}	163.3 F g^{-1} @ 1 A g^{-1}	44.45 W h kg^{-1}/0.70 kW kg^{-1}	85.1% capacitance retention after 5000 cycles @ 5 A g^{-1}	116
P-doped $NiCo_2S_{4-x}$ nanotubes	1806.4C g^{-1} @ 1 A g^{-1}	186.1 F g^{-1} @ 1 A g^{-1}	68.2 W h kg^{-1}/0.80 kW kg^{-1}	97% capacitance retention after 10 000 cycles @ 30 A g^{-1}	19
NiMn-LDH@$NiCo_2S_4$ nanotubes	1018C g^{-1} @ 1 A g^{-1}	193.0 F g^{-1} @ 0.5 A g^{-1}	60.3 W h kg^{-1}/0.38 kW kg^{-1}	86.4% capacitance retention after 10 000 cycles @ 10 A g^{-1}	74
$CoNi_2S_4$ microspheres	1836.6 F g^{-1} @ 1 A g^{-1}	100.7 F g^{-1} @ 1 A g^{-1}	38.9 W h kg^{-1}/0.85 kW kg^{-1}	101.2% capacitance retention after 50 000 cycles @ 5 A g^{-1}	106
Ag@$Ni_{0.67}Co_{0.33}S$ forest-like nanostructures	296.4 mA h g^{-1} @ 2 mA cm^{-2}	1104.14 mF cm^{-2} @ 5 mA cm^{-2}	0.36 mW h cm^{-2}/3.81 mW cm^{-2}	83.6% capacitance retention after 8000 cycles @ 20 mA cm^{-2}	44

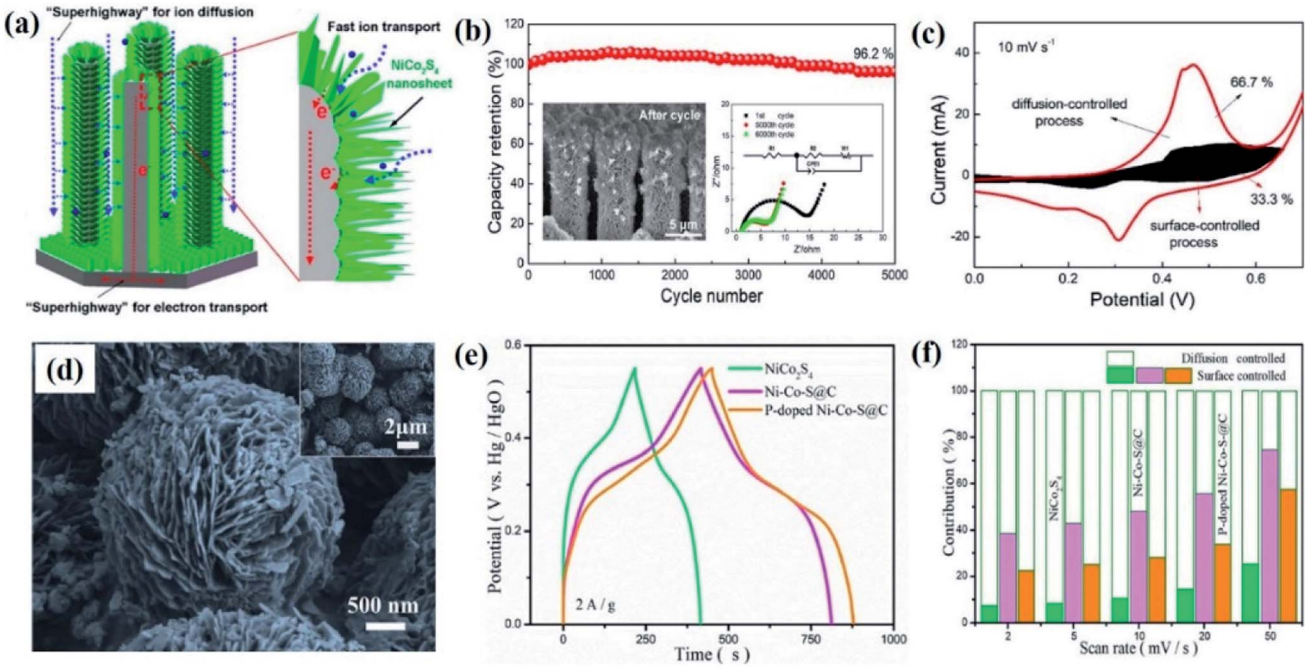

Fig. 6 Schematic diagram (a) and electrochemical performance (b and c) of $NiCo_2S_4$ nanosheets @ Ni column arrays.[53] SEM image (d) and electrochemical performance (e and f) of P-doped Ni–Co–S@C hierarchical structures.[104] Reproduced from ref. 22 with permission from American Chemical Society. Reproduced from ref. 78 with permission from Elsevier.

and surface redox processes (Fig. 6f).[44,81,106–109] However, we find that the contribution ratio of these two kinds of electrochemical behavior for NCSs is significantly influenced by the micro-/nano-structures of NCSs. The electrochemical performance of four types of $NiCo_2S_4$ hierarchical structures assembled from similar nanorod building blocks was investigated,[110] and it was

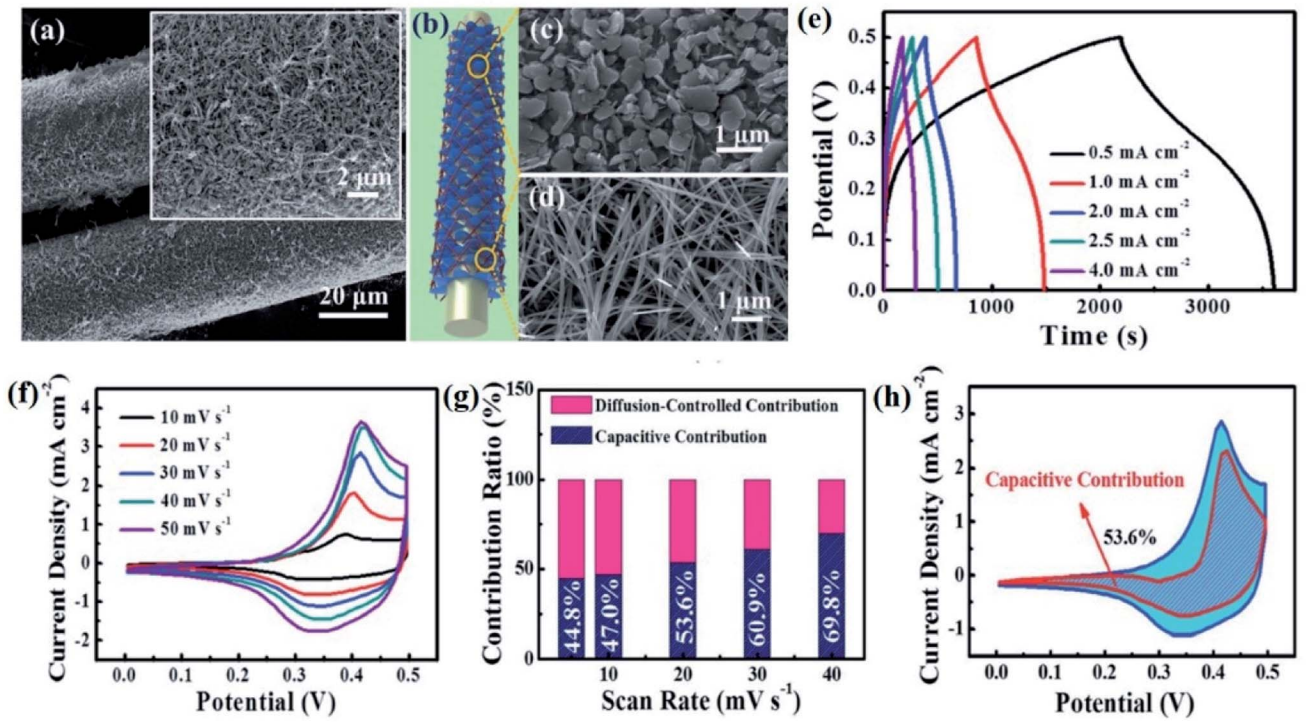

Fig. 7 SEM images (a, c and d), schematic diagram (b) and electrochemical performance (e–h) of $NiCo_2S_4$/MgS composites.[59] Reproduced from ref. 28 with permission from the Royal Society of Chemistry.

Table 2 Performance of some representative NCS-based materials in different kinds of batteries

Materials	Specific capacity	Cycling stability	Remarks	Ref.
Li-ion batteries				
$NiCo_2S_4/SnS_2$ hollow spheres (anode)	1260 mA h g^{-1} @ 0.1 A g^{-1}	627 mA h g^{-1} @ 0.5 A g^{-1} after 300 cycles	99 mA h g^{-1} @ 0.1 A g^{-1} within 2.0–5.0 V (full cells with NMC111 cathodes and $NiCo_2S_4/SnS_2$ anodes)	61
$NiCo_2S_4$@C hollow microspheres (anode)	1946.7 mA h g^{-1} @ 0.2 A g^{-1}	1242.8 mA h g^{-1} @ 2 A g^{-1} after 1000 cycles	Multi-shelled $NiCo_2S_4$ hollow microspheres were obtained by a multi-step method with solvothermal reactions, direct pyrolysis under air atmosphere and calcination in Ar/H_2S gas	126
$NiCo_2S_4$ hollow nanowires (anode)	1437.9 mA h g^{-1} @ 0.5 A g^{-1}	1198 mA h g^{-1} @ 0.5 A g^{-1} after 500 cycles	Chitin-derived N-doped carbon was used as a 3D substrate to support $NiCo_2S_4$ nanowires	18
Na-ion batteries				
$NiCo_2S_4$ @ N-doped carbon nanoparticles (anode)	742.2 mA h g^{-1} @ 0.2 A g^{-1}	395.6 mA h g^{-1} @ 6 A g^{-1} after 5000 cycles	Ether-based electrolyte: sodium trifluoromethanesulfonate ($NaCF_3SO_3$)/ diethylene glycol dimethyl ether (DEGDME)	120
Flower-like $NiCo_2S_4$ structures (anode)	748 mA h g^{-1} @ 0.1 A g^{-1}	376 mA h g^{-1} @ 2 A g^{-1} after 500 cycles	The capacitance contribution is up to 89% of total capacity @ 2 mV s^{-1}	82
$(Co_{0.5}Ni_{0.5})_9S_8$ @ N-doped carbon hollow spheres (anode)	945.1 mA h g^{-1} @ 0.1 A g^{-1}	723.7 mA h g^{-1} @ 1 A g^{-1} after 100 cycles	847.5 mA h g^{-1} @ 0.5 A g^{-1} within 0.01–3.7 V (full cells with $Na_3V_2(PO_4)_3$@C cathodes and $(Co_{0.5}Ni_{0.5})_9S_8$/N–C anodes)	40
Zn-ion batteries				
NiCoP/$NiCo_2S_4$ nanosheets (cathode)	251.1 mA h g^{-1} @ 10 A g^{-1}; 190.3 mA h g^{-1} @ 50 A g^{-1}	96.9% capacity retention @ 100 mV s^{-1} after 5000 cycles for full cells	265.1 mA h g^{-1} @ 5 A g^{-1} at 1.7 V (full cells with NiCoP/$NiCo_2S_4$ cathodes and Zn anodes)	127
$NiCo_2S_{4-x}$ nanotubes @ carbon cloth (cathode)	298.3 mA h g^{-1} @ 0.5 A g^{-1}	144.4 mA h g^{-1} @ 5.0 A g^{-1} after 1000 cycles (85% retention)	146.3 mA h g^{-1} @ 5 A g^{-1} and 84.7% retention after 1500 cycles (flexible solid-state $NiCo_2S_{4-x}$@CC//Zn@CC with a sodium polyacrylate hydrogel electrolyte)	34
Li–S batteries				
$NiCo_2S_4$ nanosheets @ carbon textile (CT) (cathode)	1600 mA h g^{-1} @ 0.1C	836 mA h g^{-1} @ 0.5C after 500 cycles (0.018% per cycle)	$NiCo_2S_4$ @ CT can be as a bifunctional interlayer for the S@MWCNT cathode with higher adsorptive ability for polysulfides	35
Hollow acicular-like $NiCo_2S_4$ microspheres (cathode)	1387 mA h g^{-1} @ 0.2C	543 mA h g^{-1} @ 2C after 500 cycles (0.06% per cycle)	A flexible Li–S battery with a sulfur loading of 8.9 mg cm^{-2} has a capacity of 720 mA h g^{-1} (6.52 mA h cm^{-2}) after 65 cycles at 0.1C	128
$NiCo_2S_{4-x}$ hollow microspheres (cathode)	1304.5 mA h g^{-1} @ 0.2C; 628.9 mA h g^{-1} @ 5C	598.2 mA h g^{-1} @ 1C after 500 cycles (0.0754% per cycle)	$NiCo_2S_{4-x}$ has strong chemical adsorption ability toward LiPSs	23
Zn–air batteries				
$(Ni,Co)S_2$ nanosheets (cathode)	Specific capacity: 842 mA h g_{Zn}^{-1} @ 5 mA cm^{-2}; charge/discharge voltage gap: 0.45 V @ 2 mA cm^{-2}; peak power density: 153.5 mW cm^{-2}	480 h @ 2 mA cm^{-2}	Cell charge/discharge voltage: 1.71/1.26 V @ 10 mA cm^{-2}	129

Table 2 (*Contd.*)

Materials	Specific capacity	Cycling stability	Remarks	Ref.
$NiCo_2S_4$ nanoparticles @ carbon nitrogen nanosheets (cathode)	Specific capacity: 801 mA h g_{Zn}^{-1} @ 10 mA cm^{-2}; charge/discharge voltage gap: 0.69 V @ 10 mA cm^{-2}; energy density: 1025 W h kg^{-2}	180 h @ 10 mA cm^{-2} (1000 cycles)	Cell charge/discharge voltage: 1.94/1.25 V @ 10 mA cm^{-2}	78
Li–O_2 batteries				
$NiCo_2S_4$ nanorods @ carbon textile (cathode)	Specific capacity: 4506 mA h g^{-1} @ 750 mA g^{-1}; charge/discharge voltage gap: 0.69 V @ 10 mA cm^{-2}; energy density: 1025 W h kg^{-2}	500 cycles with a cut-off capacity of 1000 mA h g^{-1} @ 500 mA g^{-1}	Charge overpotential: 1.17 V	83
$NiCo_2S_4$ nanoflakes/S-doped carbon nanosheets (cathode)	Specific capacity: 14 173 mA h g^{-1} @ 150 mA g^{-1}; charge/discharge voltage gap: 0.69 V @ 10 mA cm^{-2}; energy density: 1025 W h kg^{-2}	1704 h with a limited specific capacity of 1000 mA h g^{-1} @ 150 mA g^{-1}	Initial overall overpotential: 1.27 V with 1.01 and 0.26 V at charge and discharge stages (1.01/0.26 V) with 68% round-trip efficiency	130

indicated that the hat/flower-like structures with a compact packaging way showed unclear CV redox peaks and GCD discharge platforms, suggesting that the diffusion-controlled process was limited and the capacity was mainly from the surface electrochemical process. In contrast, sphere/brush-like structures with a loose and orderly assembly way presented more obvious CV redox peaks and GCD discharge platforms, revealing a higher utilization of active materials from the increased contribution of diffusion-controlled faradaic reactions in the inner part of the electrode, and thus they had larger capacity.[110] Moreover, NCSs and their composites are commonly *in situ* grown on planar substrates (*e.g.*, carbon cloth, Ni foam and metal meshes), and they usually show clear battery-like behavior,[58,81] but when the planar substrates are changed into ultrathin metal wires with a diameter on a scale of tens of micrometers and a high aspect ratio (Fig. 7a–d), clear CV redox peaks and GCD discharge platforms disappear (Fig. 7e and f), and most capacity is from the surface pseudocapacitance because of the relatively large surface area of ultrathin wires (Fig. 7g and h).[59] Therefore, it is possible to modify NCS electrodes on different aspects (*e.g.*, components, morphologies, substrates and so on) to achieve high-performance electrochemical energy storage devices.

2.2. Batteries

In recent years, NCSs have also been employed as effective electrode materials in other electrochemical energy storage devices (Table 2), such as Li/Na/Zn-ion, Li–S, Li–O_2 and Zn–air batteries, similarly because of their intrinsic properties of high electrochemical activity stemming from their rich redox reactions with multi-valence states and relatively high electrical conductivity with the synergetic effect from Ni and Co atoms (Fig. 5). The theoretical capacity of NCSs in Li-ion batteries is 703 mA h g^{-1}.[1] For example, $NiCo_2S_4$ hollow nanowires (Fig. 8a) were uniformly grown on a 3D N-doped carbon nanosheet substrate derived from a bio-polymer of Chitin (poly(*b*-(1,4)-*N*-acetyl-D-glucosamine)),[18] which exhibited attractive long-term cycling stability with a revisable capacity of 1198 mA h g^{-1} at 500 mA g^{-1} after 500 cycles (Fig. 8b). Besides, $(Co_{0.5}Ni_{0.5})_9S_8$ hollow microspheres (Fig. 8c) were converted from the Ni–Co metal–organic framework (Ni–Co-MOF) and then modified with N-doped carbon (N–C).[40] When applied as the anode in Na-ion batteries with $Na_3V_2(PO_4)_3$@C as the cathode, the full cells delivered a capacity of 737.6 mA h g^{-1} at 0.5 A g^{-1} within 0.01–3.7 V after 50 cycles. It was found that the composite electrodes had a hybrid electrochemical charge storage behavior and the pseudocapacitive contribution was up to 88.8% at 1 mV s^{-1} (Fig. 8d). In addition, $NiCo_2S_4$ porous nanoneedle arrays were *in situ* grown on N/S co-doped carbon cloth and displayed high sulfur loading capability due to the rich mesoporous structure and a great ability to absorb and convert polysulfide intermediates owing to the high electronic conductivity and catalytic activity.[117] Therefore, NCS-based materials are as well promising for Li–S batteries.

Recently, besides the *ex situ* measurement ways,[118] *in situ* characterization methods (*e.g.*, *in situ* X-ray diffraction (XRD),

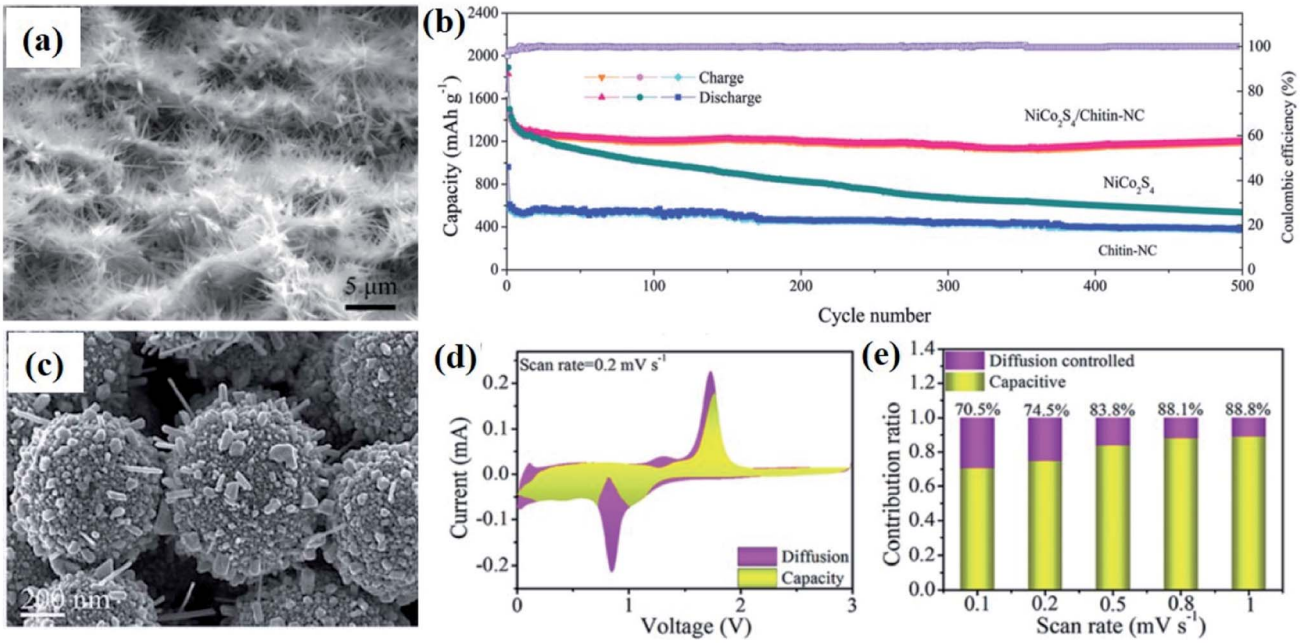

Fig. 8 SEM image (a) and cycling performance (b) of $NiCo_2S_4$/N-doped carbon.[18] SEM image (c) and capacitive contribution (d and e) of $(Co_{0.5}Ni_{0.5})_9S_8$/N-doped carbon.[40] Reproduced from ref. 49 and 12 with permission from the Royal Society of Chemistry.

photoluminescence (PL) and electrochemical impedance spectroscopy (EIS)) have been extensively developed to reveal more details about the charge storage processes for batteries. Thus, some studies have also reported the *in situ* characterization and analysis of the working mechanism of NCSs in Li/Na-ion batteries.[41,66,119–122] For example, *in situ* XRD of the $NiCo_2S_4$@CNT electrodes in Li/Na-ion batteries showed that in the first discharge process with Li/Na ion intercalation, phase change occurred with the formation of Ni/Co particles, Li_2S and Na_2S, while in the charge process, NiS and CoS would generate due to the deintercalation of Li/Na ions (Fig. 9).[66] In addition, the *in situ* EIS analysis of the interfacial properties and charge transfer resistance of $NiCo_2S_4$@carbon electrodes also confirmed the phase change with the conversion of $NiCo_2S_4$ into NiS_x and CoS_x after 200 cycles.[120] The participation of carbon materials enabled the improvement of the electrical conductivity and ensured the high reversibility of structural and phase transition of $NiCo_2S_4$ during charge/discharge cycles, thus enhancing the stability of NCS-based batteries.[66,120] Therefore, it will be very beneficial to deeply

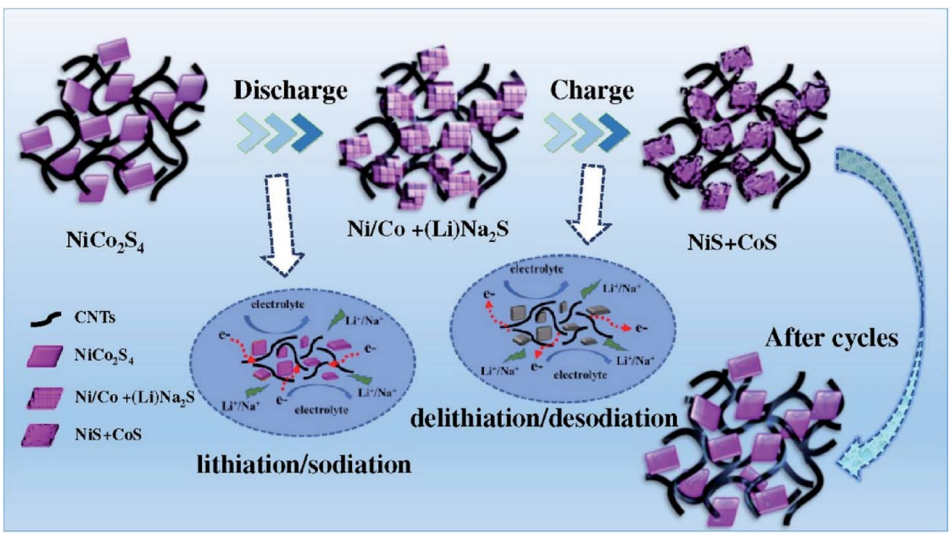

Fig. 9 Schematic diagram of the charge storage mechanism of $NiCo_2S_4$@CNT electrodes in Li/Na-ion batteries.[66] Reproduced from ref. 53 with permission from Elsevier.

Table 3 Performance of different NCS-based catalysts for water splitting

Catalyst	Overpotential of the OER	Overpotential of the HER	Water splitting	Electrolyte	Stability	Ref.
Core–shell $NiCo_2S_4$ nanorods	200 mV vs. 330 mV (IrO_2) @ 40 mA cm^{-2}	190 mV @ 10 mA cm^{-2}	1.57 V vs. 1.54 V (IrO_2/C–Pt/C) @ 10 mA cm^{-2}	1.0 M KOH	12 h	141
$NiCo_2S_4$@$Ni_3V_2O_8$	290 mV vs. 320 mV (IrO_2) @ 35 mA cm^{-2}	—	—	1.0 M KOH	10 h	132
$NiCo_2S_4$ nanorod arrays	220 mV vs. ~320 mV (IrO_2) @ 30 mA cm^{-2}	222 mV vs. ~30 mV (Pt/C) @ 30 mA cm^{-2}	1.64 V @ 20 mA cm^{-2}	1.0 M KOH	18 h	142
$NiCo_2S_4$ nanoflakes	319 mV vs. ~404 mV ($NiCo_2O_4$) @ 100 mA cm^{-2}	169 mV vs. ~238 mV ($NiCo_2O_4$) @ 10 mA cm^{-2}	1.61 V @ 10 mA cm^{-2}	1.0 M KOH	70 h	88
Crossed $NiCo_2S_4$ nanowires	256 mV vs. 340 mV (IrO_2) @ 40 mA cm^{-2}	193 mV vs. ~244 mV (Ni_3S_2) @ 10 mA cm^{-2}	1.59 V @ 10 mA cm^{-2}	1.0 M KOH	12 h	134
$NiCo_2S_4$ nanosheets	247 mV vs. 264 mV ($NiCo_3S_4$) @ 10 mA cm^{-2}	106 mV vs. ~181 mV ($NiCo_3S_4$) @ 10 mA cm^{-2}	1.62 V @ 10 mA cm^{-2}	1.0 M KOH	72 h	89
N-doped carbon–$NiCo_2S_4$ hollow nanotubes	280 mV vs. ~290 mV (IrO_2) @ 10 mA cm^{-2}	183 mV vs. ~214 mV ($NiCo_2S_4$) @ 10 mA cm^{-2}	1.60 V @ 10 mA cm^{-2}	1.0 M KOH	15 h	135
Carbon dots/$NiCo_2S_4$/Ni_3S_2 nanorods	116 mV @ 10 mA cm^{-2}	127 mV @ 10 mA cm^{-2}	1.50 V @ 10 mA cm^{-2}	1.0 M KOH	12 h	131
$NiCo_2S_4$@N,S co-doped reduced graphene oxides	253 mV vs. 267.8 mV (RuO_2) @ 10 mA cm^{-2}	92.7 mV vs. 61.9 mV (Pt/C) @ 10 mA cm^{-2}	1.58 V in 1 M KOH and 1.907 V in 1 M phosphate buffer solution @10 mA cm^{-2}	1.0 M KOH	10 h	136

elucidate the working mechanism and key processes in electrochemical energy storage devices by combining *in situ* and *ex situ* characterization methods, ultimately guiding the design of more high-performance devices.

For the applications of Zn–air and Li–O_2 batteries, the electrocatalytic activity and durability in the oxygen reduction reactions (ORR) for the discharge process and the oxygen evolution reactions (OER) for the charge process are very essential for advanced cathode electrode materials. Many studies have confirmed that NCSs are feasible for metal–oxygen batteries as a class of bifunctional cathodes,[69,78,123–125] still due to their excellent electrochemical activity and reversibility in redox reactions. For example, $NiCo_2S_4$ nanoparticles were integrated with carbon nitrogen nanosheets and demonstrated efficient bifunctional electrocatalytic performance (*i.e.*, a positive half-wave potential of 0.83 V for the ORR and a low overpotential of 360 mV at 10 mA cm^{-2} for the OER).[78] The corresponding Zn–air batteries showed a maximum power density of 92 mW cm^{-2}, a capacity of 801 mA h g^{-1}, an energy density of 1025 W h kg^{-1}, and outstanding cycling durability for 180 h with 1000 cycles at 10 mA cm^{-2}, which were comparable or superior to those (106 mW cm^{-2}, 759 mA h g^{-1}, 925 W h kg^{-1}, and 69 h) of the commercial Pt/C–RuO_2-based one.

3. Applications of NCSs in water splitting

Nowadays, electrochemical water splitting is widely recognized as one of the most prospective strategies to generate hydrogen (Fig. 10a), which is mostly accepted as an ideal energy choice to substitute for conversional fossil fuels. There are two important processes involved in the electrocatalysis of water, that is, the hydrogen evolution reaction (HER) and oxygen evolution reaction (OER), which require highly active electrocatalysts to overcome the large overpotential (1.6–2.0 V) of these reactions. To date, IrO_2 and Pt have been considered as the best catalysts for the OER and HER; nevertheless, the high price of noble metals restricts their large-scale applications. Thus, alternative electrocatalysts with low cost and high activity have attracted much attention. Because of the co-existence of Ni and Co with rich active sites from the redox couples (*i.e.*, Co^{3+}/Co^{2+} and Ni^{3+}/Ni^{2+}) in crystal structures, NCSs show higher conductivity and catalytic capability than binary sulfides (Fig. 10b–d), and then have been applied in electrocatalytic water splitting as a promising type of bifunctional catalyst (Fig. 10a and Table 3).[131–133]

Much effort has been devoted to the rational engineering of the components and nanostructures of NCSs,[88,89,131,132,134,135] in order to further enlarge their reactive surface areas, improve their electrical conductivity and enhance their catalytic stability, ultimately synergistically strengthening their electrocatalytic performance. For example, nanorod assembled $NiCo_2S_4$ microspheres were *in situ* planted onto N,S co-doped reduced graphene oxides,[136] which exhibited outstanding bifunctional electrocatalytic ability in the HER and OER with a low cell voltage of 1.58 V in 1 M KOH for overall water splitting. More impressively, they also had electrocatalytic capability in

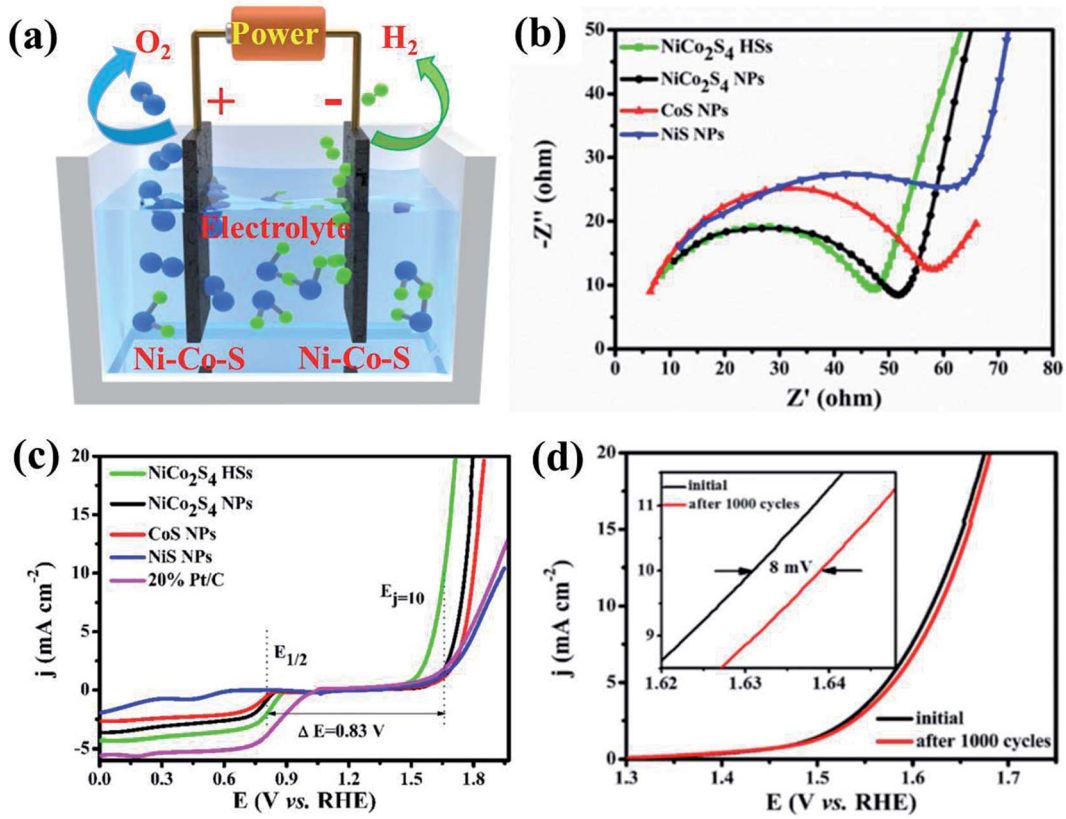

Fig. 10 (a) Schematic diagram of the water splitting process based on NCSs. (b) Nyquist plots, and (c) oxygen reduction reaction and oxygen evolution reaction curves of different catalysts. (d) Stability tests of the NCS catalyst.[133] Reproduced from ref. 133 with permission from American Chemical Society.

a neutral electrolyte (1 M phosphate buffer solution) with a cell voltage of 1.91 V, which is very meaningful to avoid the corrosion of devices from alkaline electrolytes and reduce the operating cost for practical applications. Besides, $NiCo_2O_4$, $NiCo_2S_4$ and $NiCo_2Se_4$ nanosheets were separately grown on conductive carbon papers to compare their behavior in electrocatalytic water splitting.[137] For the HER at 10 mA cm^{-2}, the overpotential value for $NiCo_2Se_4$ (56 mV) was relatively lower than those of $NiCo_2S_4$ (87 mV) and $NiCo_2O_4$ (141 mV), but still slightly higher than that of Pt/C (41 mV). However, for the OER at 25 mA cm^{-2}, $NiCo_2S_4$ possessed the lowest overpotential value of 251 mV as compared to other materials (*i.e.*, $NiCo_2O_4$: 372 mV; $NiCo_2Se_4$: 321 mV; IrO_2/C: 358 mV). Accordingly, $NiCo_2S_4$ and $NiCo_2Se_4$ were employed as the anode and cathode for overall water splitting, respectively, yielding a low cell voltage of 1.51 V for driving the generation of H_2 and O_2 bubbles at 10 mA cm^{-2}. Theoretical calculation unraveled that the center position of the d band for electrodes was closely related to the electrocatalytic activity. It was found that $NiCo_2S_4$ and $NiCo_2Se_4$ had the d band center closer to the Fermi level, suggesting increased unoccupied orbitals due to the existence of S and Se, and the upward movement of the antibonding d state with strengthened adsorption interaction with reactive species (*e.g.*, H_2O and H*) for enhanced electrocatalytic performance.[137]

In addition, due to their excellent electrocatalytic activity, NCSs have also been proved to be effective electrocatalysts for the alkaline urea electrooxidation reaction in urea fuel cells, which are accepted as one promising strategy to use urea from wastewater to produce electricity and hydrogen.[52,138–140] For example, $NiCo_2S_4$ nanowires were *in situ* grown on a carbon sponge, which showed great electrocatalytic performance with a large electrochemically active surface area of 330.7 cm^{-2} and a low activation energy of 15.3 kJ mol^{-1} towards the urea oxidation reaction.[140] It is believed that the excellent electrocatalytic properties of NCSs will make them have good application prospects in other electrocatalysis fields.

4. Applications of NCSs in solar cells

NCSs are frequently used as counter electrode materials in dye-sensitized solar cells (DSCs) and quantum dot-sensitized solar cells (QDSCs).[84,143–146] In DSCs and QDSCs, counter electrodes (CEs) play an important role in collecting electrons from the

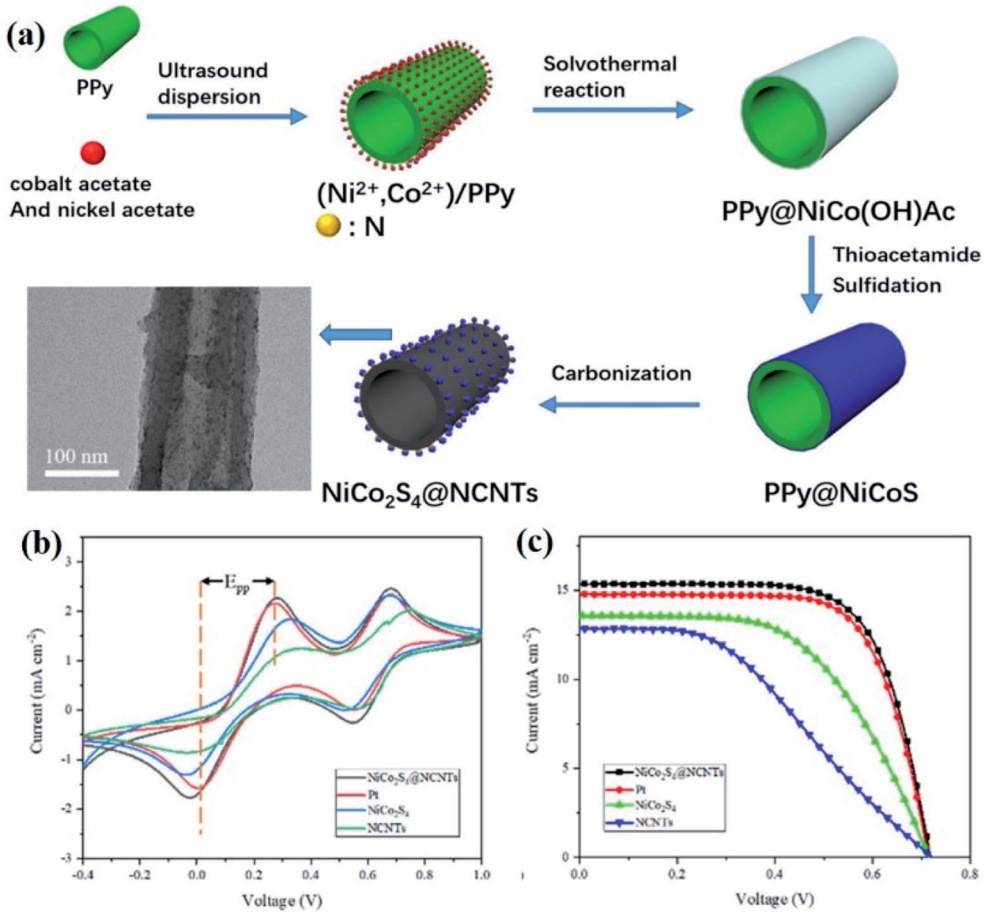

Fig. 11 Schematic diagram of the synthesis process and TEM image for the $NiCo_2S_4$ quantum dots @ CNTs (a), and CV curves (b) and *J*–*V* curves of DSCs (c) for different counter electrodes.[147] Reproduced from ref. 110 with permission from American Chemical Society.

external circuit to electro-catalyze the reduction of the electrolyte and thus realize continuous photoelectric conversion. For DSCs, Pt is an ideal choice as the CE due to its excellent electrocatalytic ability for the reduction of iodide/triiodide (I^-/I_3^-) redox electrolytes.[145] However, the high cost of Pt inspires people to develop cheaper alternatives. For QDSCs, Pt is inefficient for the reduction of polysulfide redox electrolytes because of the strong adsorption of sulfur atoms onto the Pt surface to reduce its conductivity and reduction ability.[143] Therefore, effective CE materials have been intensively developed, including carbon-based materials, metal sulfides and so on.

Among them, NCS-based materials are expected to be promising CE alternatives because they provide rich redox reactions and relatively high conductivity from the synergetic effect of Ni and Co atoms. For instance, $NiCo_2S_4$ quantum dots (QDs) were decorated onto the surface of nitrogen-doped carbon nanotubes (N-CNTs) as CEs for DSCs (Fig. 11a).[147] It was found that such CEs showed comparable electrocatalytic performance to Pt (Fig. 11b and c; photoelectric conversion efficiency of DSCs: 7.65% for $NiCo_2S_4$@N-CNTs *vs.* 7.39% for Pt). This was mainly because of the uniform distribution of $NiCo_2S_4$ QDs on CNTs for abundant reaction sites, the special 1D channels of CNTs for rapid charge transport and ion diffusion, and the strong metal–nitrogen bonding between $NiCo_2S_4$ QDs and CNTs due to the nitrogen doping.

5. Applications of NCSs in photocatalysis

Recently, metal sulfides have been widely applied in photocatalysis,[148–150] and NCSs are also introduced into the photocatalytic system mainly due to their great photoelectric conductivity and p-type semiconductor characteristics (E_g = ~2.5 eV). For example, NCS@MXene composites were prepared as a photocatalyst and exhibited great photocatalytic activity and stability in the degradation of rhodamine B under visible light conditions.[86] Besides, $NiCo_2S_4$/CdS (Fig. 12),[87] $NiCo_2S_4$@-$Zn_{0.5}Cd_{0.5}S$,[151] and $NiCo_2S_4$/g-C_3N_4 (ref. 152) co-catalysts have been fabricated and proved to be efficient in visible-light-irradiation photocatalytic hydrogen generation because the

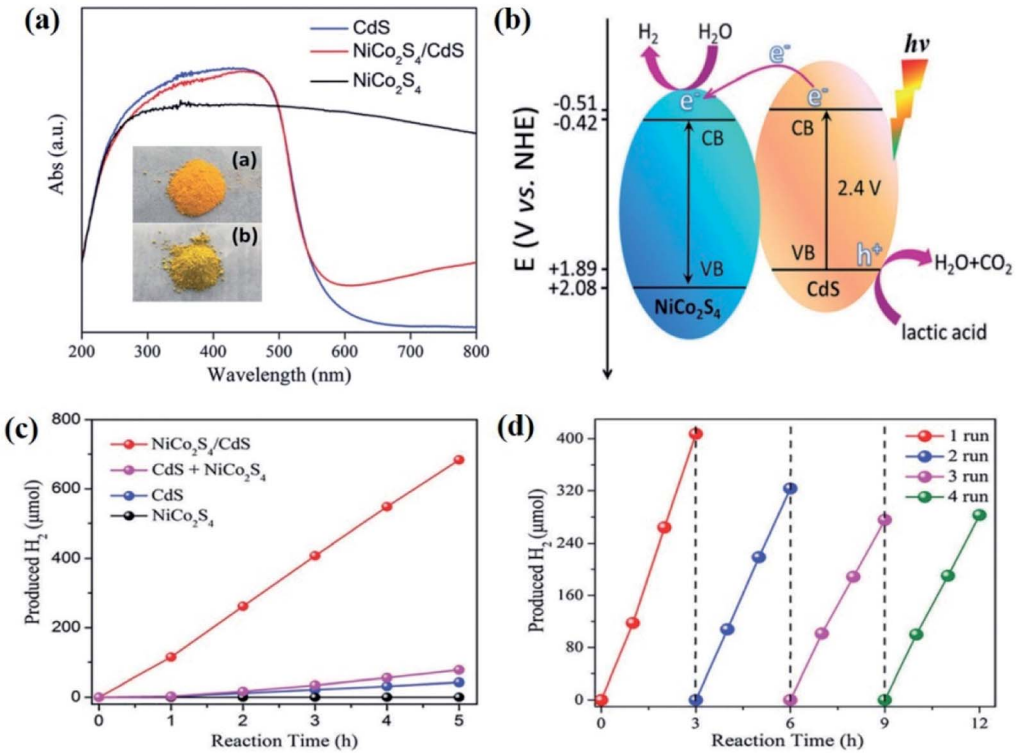

Fig. 12 Light absorption plots and real pictures (a), and H_2 production (c) of different photocatalysis (a), and schematic diagram of the working process (b) and cycling performance (d) for photocatalytic H_2 generation by $NiCo_2S_4$/CdS (b).[87] Reproduced from ref. 55 with permission from the Royal Society of Chemistry.

participation of NCSs is able to significantly enhance the carrier separation and migration due to the heterojunction formation in the co-catalysts.

Moreover, $NiCo_2S_4$ micro-particles were synthesized *via* a solvothermal method and then applied as noble-metal-free catalysts in the CO_2 photoreduction system.[122] Photocatalytic CO_2 reduction is considered as a promising strategy to realize the direct conversion of solar energy into special chemicals (*e.g.*, CO) with the advantages of using renewable solar energy and alleviating the climate change from CO_2 emission. Here, the $NiCo_2S_4$ photocatalyst showed considerable activity for visible-light CO_2 reduction, yielding a production rate of 43.5 μmol mg^{-1} h^{-1} for CO. *In situ* steady-state photoluminescence and transient photocurrent tests indicated that the $NiCo_2S_4$ catalyst enabled the reduction of the recombination and the acceleration of the transport of photo-generated charges during the CO_2 reduction process.[122]

6. Applications of NCSs in sensors

The accurate detection of glucose concentration in various sources (*e.g.*, human blood, foods and pharmaceuticals) is essential and necessary for personal healthcare, diagnosis and therapy of diseases (*e.g.*, diabetes mellitus), drug analysis, food monitoring and so on.[153] It requires that glucose-monitoring devices should be efficient, reliable, low-cost, and simple. Enzyme-immobilized electrodes are widely used as glucose sensors due to their high sensitivity. However, such glucose sensors demand complex operating conditions for the attachment of enzymes onto the electrode surface, and the biomass enzymes are usually unstable under high temperature, humidity or acidity and alkalinity conditions.[90]

To address these problems, enzyme-free glucose sensors based on various inorganic materials (*e.g.*, metal nanoparticles, metal oxides, sulfides, *etc.*) have been developed recently. NCSs and their composites with different structures (*e.g.*, $NiCo_2S_4$ nanosheets/nanowires/hollow spheres,[90,154,155] and NiS/CoS/$NiCo_2S_4$ micro-flowers[156]) are also considered as an optimal choice for non-enzymatic glucose sensors based on their good electrocatalytic activity toward glucose oxidation. Moreover, they have several advantages, such as facile synthesis, high sensitivity, great stability and low cost. For example, flower-like $NiCo_2S_4$ structures constructed from many interlaced nanosheets were simply electrodeposited onto Ni-coated cellulose filter paper (Fig. 13a),[153] which showed satisfactory sensing performance for glucose detection (Fig. 13b–e), including a wide linear range (0.5 μM to 6 mM; Fig. 13d) for the glucose content, considerable sensitivity (283 μA mM^{-1} cm^{-2}), a low detection limit (50 nM), great selectivity (Fig. 13e), excellent repeatability and electrochemical stability.

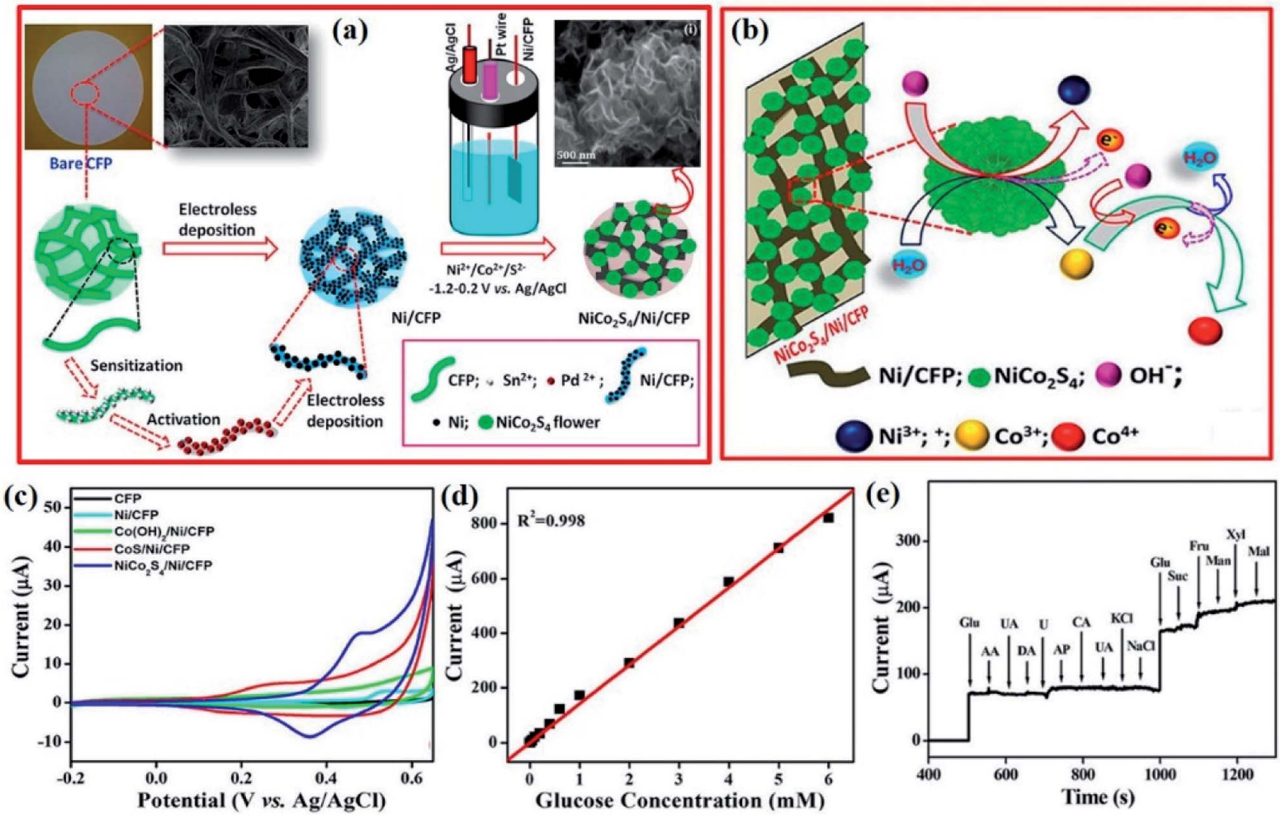

Fig. 13 Schematic diagrams of the preparation process (a) and sensing process (b), and glucose sensing performance: (c) CV curves in 2 mM glucose and 0.1 M NaOH at 20 mV s^{-1}, (d) linear properties and (e) selectivity with interfering species (AA, UA, DA, U, AP, CA, KCl, NaCl, *etc.*) and glucose (Glu) for $NiCo_2S_4$/Ni/cellulose filter paper.[153] Reproduced from ref. 113 with permission from American Chemical Society.

Similarly, the excellent electrocatalytic capability of NCSs also endows them with great sensing performance for the detection of other substances (*e.g.*, sulfadimethoxine (SDM)[54] and pyrimethanil[157]). It was reported that a $NiCo_2S_4$@N/S-doped CeO_2 composite was able to be an effective signal amplification label in a DNA aptasensor for detecting SDM, which is widely used for the veterinary treatment of coccidiosis and other bacterial infections but harmful to organisms even at a low concentration. This was because the composite had great electrocatalytic performance for the oxygen reduction reaction, and thus excellent electrocatalytic amplification for SDM detection with high sensitivity and selection.[54] In addition, NCS-based materials (*e.g.*, $NiCo_2S_4$/reduced graphene oxide nanosheets) also can act as gas sensors for ethanol monitoring by recording the resistance change of sensing materials. This is mainly due to the adsorption of O_2 molecules on the electrode surface and the reaction between the ethanol molecules and the adsorbed O_2 molecules will change the electrode resistance.[158]

7. Applications of NCSs in microwave absorption

With the improvement of science and technology, more and more electronic products come into our daily life, while the accompanying electromagnetic radiation and interference will affect the human health, influence the normal operation of electronic devices, and even threaten the national defense safety. Thus, a variety of microwave absorption materials have been extensively studied in order to effectively absorb and then transform electromagnetic microwaves into other types of energy (*e.g.*, thermal energy; Fig. 14a).[159] Ideal microwave absorbers should have a high absorption capacity, a wide absorption frequency range, low cost and light weight. Carbon-based materials (*e.g.*, carbon nanotubes, graphene and porous carbon materials) have been widely used to absorb microwaves primarily due to their tunable dielectric properties, large specific surface areas, light weight and high chemical stability.[160]

Recently, NCSs have also been considered to be a potential microwave absorption material owing to their great magnetic loss performance.[161,162] For example, $NiCo_2S_4$ nanosheets or microspheres were combined with carbon materials (*e.g.*, biomass derived carbon mesoporous[91,163] and hollow carbon microspheres[164]) to achieve excellent microwave absorption capability (Fig. 14b), such as a minimum reflection loss value of −64.74 dB and a wide absorption range from 9.22 to 14.48 GHz.[163] It was found that the assistance of $NiCo_2S_4$ in the biomass-derived carbon composite was able to improve the impedance matching and the attenuation constant for strong microwave absorption.[91] Therefore, it is promising to develop

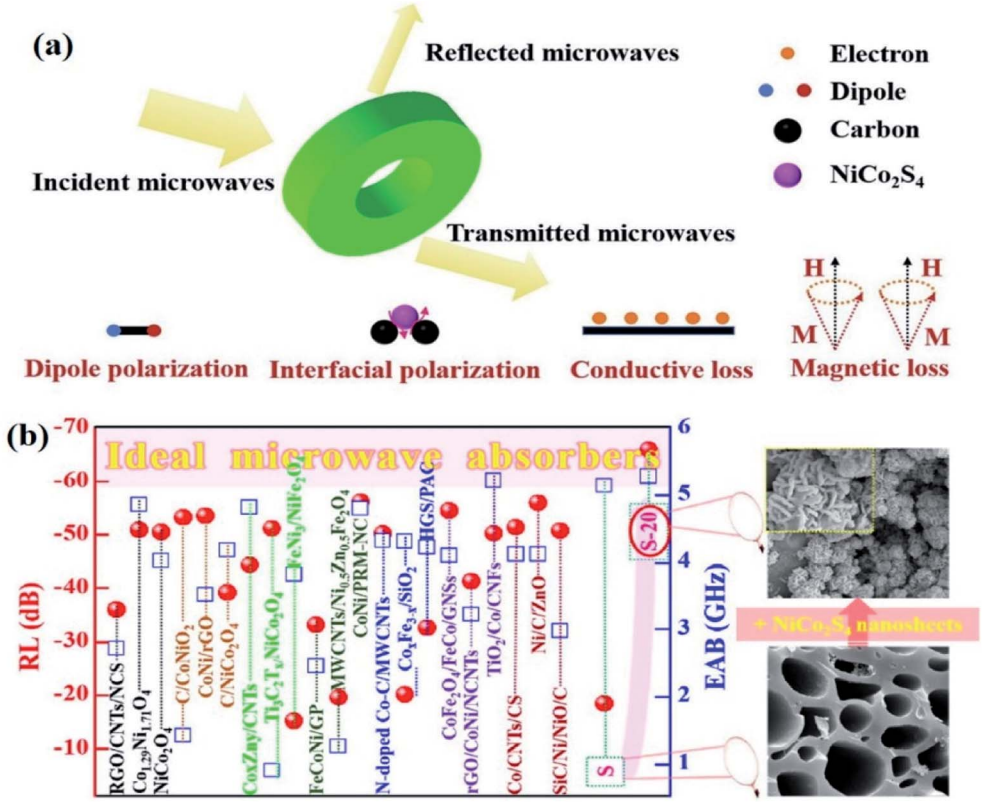

Fig. 14 Proposed microwave absorption mechanism of NCS-based materials (a) and comparison of microwave absorption ability among different materials (b).[163] Reproduced from ref. 121 with permission from Elsevier.

highly efficient and low-cost microwave absorbers based on NCS materials.

8. Conclusion and prospects

In summary, NCS-based materials have been extensively studied in recent years. They possess great performances in different applications due to their intrinsic characteristics of highly reactive activity from the multivalent states of crystals, and relatively high electronic conductivity from the cooperation of Ni and Co atoms. This review summarizes the recent development of NCSs on various aspects of micro/nano-structure design, element modulation and dopants, heterojunction building and composite integration. It emphasizes the applications of NCSs in several fields, including electrochemical energy storage devices (*e.g.*, supercapacitors, Li/Na/Zn-ion batteries, and Li–S/Zn–air/Li–O_2 batteries), water splitting, DSCs/QDSCs, photocatalysis, sensors and microwave absorption. It is indicated that these important applications are all mainly based on the attractive properties of NCSs, such as relatively high conductivity, rich active sites, and tunable components.

Although much progress has been achieved on the development of NCS-based materials for different devices, these materials are still unsatisfactory to meet the requirement for practical applications. For example, the specific capacity, energy density, and stability of the corresponding energy storage devices aren't quite high. Although the energy density of NCS-based supercapacitors is higher than that of the carbon-based ones, their power density and cycling stability are reduced concurrently. Compared to other typical batteries with high energy density, NCS-based batteries are still unsatisfactory. Besides, the high self-discharge rate (10–40%/day) of NCS-based supercapacitors should be addressed for their practical applications. Similarly, the catalytic activity and cycling stability of NCSs for the applications of electrocatalysis, photocatalysis, and sensing devices also need further enhancement. In addition, the manufacturing cost, environmental compatibility, and industrial-scale preparation should be especially concerned in future. Moreover, the relationship between the microscopic characteristics of NCS materials and the macroscopic performance should be understood more for the further rational design of NCS materials.

For the performance improvement, the exploitation and construction of highly effective NCS materials concerning various aspects (*e.g.*, modulation of the element ratio, formation of efficient nanostructures, and integration of other components) are definitely required to expose abundant active surface sites, strength electronic conductivity, build fast channels for charge transfer and mass diffusion, and enhance the cycling durability of NCS-based systems. Besides, deep understand of the material behavior and working mechanisms of NCSs in different application systems is very important for their performance improvement. The combination of *ex situ* and *in*

situ characterization techniques is very useful to disclose the underlying mechanisms (*e.g.*, component conversion, structural evolution, reaction pathways, and interfacial interaction) of NCS-based applications.[41,66,119–121,165] Besides, the optimization of mathematical modeling and theoretical simulation with higher rationality and reliability is also very helpful to promote the practical applications of NCSs.[15,69,117,121,166] It is noteworthy that machine learning has been rapidly developed and widely applied in many fields, which is possibly a powerful way for the investigation of NCSs with superior performance in various applications by the purposeful design and simple, large-scale, high efficiency and low-cost preparation strategies.

Conflicts of interest

There are no conflicts to declare.

Acknowledgements

The authors gratefully acknowledge the financial support from the Shenzhen Science and Technology Program (No. JCYJ20190809161407424), the National Natural Science Foundation of China (No. 22075237), the Natural Science Foundation of Fujian Province of China (No. 2020J01007), and the Fundamental Research Funds for the Central Universities of China (No. 20720210029).

References

1 X. Chen, Q. Liu, T. Bai, W. Wang, F. He and M. Ye, *Chem. Eng. J.*, 2021, **409**, 127237.
2 B. Yan, X. Li, W. Xiao, J. Hu, L. Zhang and X. Yang, *J. Mater. Chem. A*, 2020, **8**, 17848–17882.
3 X. Zhao, F. Gong, Y. Zhao, B. Huang, D. Qian, H.-E. Wang, W. Zhang and Z. Yang, *Chem. Eng. J.*, 2020, **392**, 123675.
4 C. Miao, C. Zhou, H.-E. Wang, K. Zhu, K. Ye, Q. Wang, J. Yan, D. Cao, N. Li and G. Wang, *J. Power Sources*, 2021, **490**, 229532.
5 J. Ren, M. Shen, Z. Li, C. Yang, Y. Liang, H.-E. Wang, J. Li, N. Li and D. Qian, *J. Power Sources*, 2021, **501**, 230003.
6 J. Zhao, G. Wang, K. Cheng, K. Ye, K. Zhu, J. Yan, D. Cao and H.-E. Wang, *J. Power Sources*, 2020, **451**, 227737.
7 T. Zhu, Z. He, Y. Ren, W. Zeng, J. Mao and L. Zhu, *Sol. RRL*, 2021, **5**, 2100021.
8 G. Fu and J.-M. Lee, *J. Mater. Chem. A*, 2019, **7**, 9386–9405.
9 P. Kulkarni, S. K. Nataraj, R. G. Balakrishna, D. H. Nagaraju and M. V. Reddy, *J. Mater. Chem. A*, 2017, **5**, 22040–22094.
10 T. Chen, S. Wei and Z. Wang, *ChemPlusChem*, 2020, **85**, 43–56.
11 T.-F. Yi, J.-J. Pan, T.-T. Wei, Y. Li and G. Cao, *Nano Today*, 2020, **33**, 100894.
12 X. Xu, H. Liang, F. Ming, Z. Qi, Y. Xie and Z. Wang, *ACS Catal.*, 2017, **7**, 6394–6399.
13 X. Wang, X. Xu, J. Chen and Q. Wang, *ACS Sustainable Chem. Eng.*, 2019, **7**, 12331–12339.
14 S. Hyun and S. Shanmugam, *ACS Omega*, 2018, **3**, 8621–8630.
15 H. Zhang, J. Liu, X. Lin, T. Han, M. Cheng, J. Long and J. Li, *J. Alloys Compd.*, 2020, **817**, 153293.
16 Q. Hu, W. Ma, G. Liang, H. Nan, X. Zheng and X. Zhang, *RSC Adv.*, 2015, **5**, 84974–84979.
17 K. Guo, Y. Ding, J. Luo and Z. Yu, *ACS Appl. Mater. Interfaces*, 2018, **10**, 19673–19681.
18 X. Wu, S. Li, B. Wang, J. Liu and M. Yu, *Chem. Commun.*, 2021, **57**, 1002–1005.
19 L. Kang, M. Zhang, J. Zhang, S. Liu, N. Zhang, W. Yao, Y. Ye, C. Luo, Z. Gong, C. Wang, X. Zhou, X. Wu and S. C. Jun, *J. Mater. Chem. A*, 2020, **8**, 24053–24064.
20 X. Wang, R. Zhou, C. Zhang, S. Xi, M. W. M. Jones, T. Tesfamichael, A. Du, K. Gui, K. Ostrikov and H. Wang, *J. Mater. Chem. A*, 2020, **8**, 9278–9291.
21 J. Wu, X. Shi, W. Song, H. Ren, C. Tan, S. Tang and X. Meng, *Nano Energy*, 2018, **45**, 439–447.
22 V. Ganesan, P. Ramasamy and J. Kim, *Int. J. Hydrogen Energy*, 2017, **42**, 5985–5992.
23 W. Wang, J. Li, Q. Jin, Y. Liu, Y. Zhang, Y. Zhao, X. Wang, A. Nurpeissova and Z. Bakenov, *ACS Appl. Energy Mater.*, 2021, **4**, 1687–1695.
24 F. Lu, M. Zhou, K. Su, T. Ye, Y. Yang, T. D. Lam, Y. Bando and X. Wang, *ACS Appl. Mater. Interfaces*, 2019, **11**, 2082–2092.
25 L. Hou, H. Hua, R. Bao, Z. Chen, C. Yang, S. Zhu, G. Pang, L. Tong, C. Yuan and X. Zhang, *ChemPlusChem*, 2016, **81**, 557–563.
26 L. Hou, R. Bao, Z. Chen, M. Rehan, L. Tong, G. Pang and C. Yuan, *Electrochim. Acta*, 2016, **214**, 76–84.
27 T. Zhu, J. Wang and G. W. Ho, *Nano Energy*, 2015, **18**, 273–282.
28 Z. Chen, X. Wang, H. Wang, H. Wang, T. Bai, F. Ren, P. Ren, H. Yan, K. Xiao and Z. Shen, *J. Alloys Compd.*, 2022, **891**, 161988.
29 J. Lin, Y. Wang, X. Zheng, H. Liang, H. Jia, J. Qi, J. Cao, J. Tu, W. Fei and J. Feng, *Dalton Trans.*, 2018, **47**, 8771–8778.
30 Y. Liu, Y. Wen, Y. Zhang, X. Wu, H. Li, H. Chen, J. Huang, G. Liu and S. Peng, *Sci. China Mater.*, 2020, **63**, 1216–1226.
31 G. Xiang, Y. Meng, G. Qu, J. Yin, B. Teng, Q. Wei and X. Xu, *Sci. Bull.*, 2020, **65**, 443–451.
32 Y. Chen, T. Liu, L. Zhang and J. Yu, *ACS Sustainable Chem. Eng.*, 2019, **7**, 11157–11165.
33 M. Chuai, K. Zhang, X. Chen, Y. Tong, H. Zhang and M. Zhang, *Chem. Eng. J.*, 2020, **381**, 122682.
34 C. Han, T. Zhang, J. Li, B. Li and Z. Lin, *Nano Energy*, 2020, **77**, 105165.
35 B. Liu, S. Huang, D. Kong, J. Hu and H. Y. Yang, *J. Mater. Chem. A*, 2019, **7**, 7604–7613.
36 N. Kurra, C. Xia, M. N. Hedhili and H. N. Alshareef, *Chem. Commun.*, 2015, **51**, 10494–10497.
37 T. Wang, B. Zhao, H. Jiang, H.-P. Yang, K. Zhang, M. M. F. Yuen, X.-Z. Fu, R. Sun and C.-P. Wong, *J. Mater. Chem. A*, 2015, **3**, 23035–23041.
38 X. Zhang, Y. Zheng, J. Zhou, W. Zheng and D. Chen, *RSC Adv.*, 2017, **7**, 13406–13415.
39 H. Chen, J. Jiang, Y. Zhao, L. Zhang, D. Guo and D. Xia, *J. Mater. Chem. A*, 2015, **3**, 428–437.

40 D. Cao, W. Kang, S. Wang, Y. Wang, K. Sun, L. Yang, X. Zhou, D. Sun and Y. Cao, *J. Mater. Chem. A*, 2019, **7**, 8268–8276.
41 S. Li, C. Li, W. K. Pang, Z. Zhao, J. Zhang, Z. Liu and D. Li, *ACS Appl. Mater. Interfaces*, 2019, **11**, 27805–27812.
42 Y. Tang, S. Chen, S. Mu, T. Chen, Y. Qiao, S. Yu and F. Gao, *ACS Appl. Mater. Interfaces*, 2016, **8**, 9721–9732.
43 N. Zhao, H. Fan, J. Ma, M. Zhang, C. Wang, H. Li, X. Jiang and X. Cao, *J. Power Sources*, 2019, **439**, 227097.
44 G. Nagaraju, S. C. Sekhar, B. Ramulu and J. S. Yu, *Small*, 2019, **15**, 1805418.
45 Y. Wen, Y. Liu, T. Wang, Z. Wang, Y. Zhang, X. Wu, X. Chen, S. Peng and D. He, *ACS Appl. Energy Mater.*, 2021, **4**, 6531–6541.
46 X. Li, Q. Li, Y. Wu, M. Rui and H. Zeng, *ACS Appl. Mater. Interfaces*, 2015, **7**, 19316–19323.
47 Y. Xu, A. Sumboja, Y. Zong and J. A. Darr, *Catal. Sci. Technol.*, 2020, **10**, 2173–2182.
48 B. Guo, T. Yang, W. Du, Q. Ma, L.-z. Zhang, S.-J. Bao, X. Li, Y. Chen and M. Xu, *J. Mater. Chem. A*, 2019, **7**, 12276–12282.
49 L. Hou, Y. Shi, S. Zhu, M. Rehan, G. Pang, X. Zhang and C. Yuan, *J. Mater. Chem. A*, 2017, **5**, 133–144.
50 Y. Jiang, X. Qian, C. Zhu, H. Liu and L. Hou, *ACS Appl. Mater. Interfaces*, 2018, **10**, 9379–9389.
51 P. Liu, Y. Liu, J. Li, M. Wang and H. Cui, *Nanoscale*, 2020, **12**, 22330–22339.
52 W. Song, M. Xu, X. Teng, Y. Niu, S. Gong, X. Liu, X. He and Z. Chen, *Nanoscale*, 2021, **13**, 1680–1688.
53 Z. Hao, X. He, H. Li, D. Trefilov, Y. Song, Y. Li, X. Fu, Y. Cui, S. Tang, H. Ge and Y. Chen, *ACS Nano*, 2020, **14**, 12719–12731.
54 L. Li, L. Yang, S. Zhang, Y. Sun, F. Li, T. Qin, X. Liu, Y. Zhou and S. Alwarappan, *J. Mater. Chem. C*, 2020, **8**, 14723–14731.
55 C. Wang, Z. Guan, Y. Shen, S. Yu, X.-Z. Fu, R. Sun and C.-P. Wong, *Chem. Eng. J.*, 2018, **346**, 193–202.
56 Y. Ouyang, H. Ye, X. Xia, X. Jiao, G. Li, S. Mutahir, L. Wang, D. Mandler, W. Lei and Q. Hao, *J. Mater. Chem. A*, 2019, **7**, 3228–3237.
57 J. Zhu, S. Tang, J. Wu, X. Shi, B. Zhu and X. Meng, *Adv. Energy Mater.*, 2017, **7**, 1601234.
58 Q. Liu, X. Hong, X. You, X. Zhang, X. Zhao, X. Chen, M. Ye and X. Liu, *Energy Storage Materials*, 2020, **24**, 541–549.
59 X. Zhang, X. Chen, T. Bai, J. Chai, X. Zhao, M. Ye, Z. Lin and X. Liu, *J. Mater. Chem. A*, 2020, **8**, 11589–11597.
60 X.-Z. Song, F.-F. Sun, Y.-L. Meng, Z.-W. Wang, Q.-F. Su and Z. Tan, *New J. Chem.*, 2019, **43**, 3601–3608.
61 H. Zhang, A. Hao, Z. Sun, X. Ning, J. Guo, Y. Lv and D. Jia, *J. Alloys Compd.*, 2020, **847**, 156505.
62 C. Zhang, M. Hou, X. Cai, J. Lin, X. Liu, R. Wang, L. Zhou, J. Gao, B. Li and L. Lai, *J. Mater. Chem. A*, 2018, **6**, 15630–15639.
63 J. Shen, J. Wu, L. Pei, M.-T. F. Rodrigues, Z. Zhang, F. Zhang, X. Zhang, P. M. Ajayan and M. Ye, *Adv. Energy Mater.*, 2016, **6**, 1600341.
64 X. Chang, W. Li, Y. Liu, M. He, X. Zheng, J. Bai and Z. Ren, *J. Colloid Interface Sci.*, 2018, **538**, 34–44.
65 L. Wan, C. He, D. Chen, J. Liu, Y. Zhang, C. Du, M. Xie and J. Chen, *Chem. Eng. J.*, 2020, **399**, 125778.
66 S. Fan, H. Liu, S. Bi, C. Gao, X. Meng and Y. Wang, *Electrochim. Acta*, 2021, **388**, 138618.
67 S.-x. Yan, S.-h. Luo, J. Feng, P.-w. Li, R. Guo, Q. Wang, Y.-h. Zhang, Y.-g. Liu and S. Bao, *Chem. Eng. J.*, 2020, **381**, 122659.
68 H. S. Lee, J. Pan, G. S. Gund and H. S. Park, *Adv. Mater. Interfaces*, 2020, **7**, 2000138.
69 W. Liu, B. Ren, W. Zhang, M. Zhang, G. Li, M. Xiao, J. Zhu, A. Yu, L. Ricardez-Sandoval and Z. Chen, *Small*, 2019, **15**, 1903610.
70 Y. Zhu, J. Li, X. Yun, G. Zhao, P. Ge, G. Zou, Y. Liu, H. Hou and X. Ji, *Nano-Micro Lett.*, 2020, **12**, 16.
71 Y. Liu, G. Jiang, Z. Huang, Q. Lu, B. Yu, U. Evariste and P. Ma, *ACS Appl. Energy Mater.*, 2019, **2**, 8079–8089.
72 X. Zhao, Q. Ma, K. Tao and L. Han, *ACS Appl. Energy Mater.*, 2021, **4**, 4199–4207.
73 X. He, Q. Liu, J. Liu, R. Li, H. Zhang, R. Chen and J. Wang, *Chem. Eng. J.*, 2017, **325**, 134–143.
74 S. Chen, C. Lu, L. Liu, M. Xu, J. Wang, Q. Deng, Z. Zeng and S. Deng, *Nanoscale*, 2020, **12**, 1852–1863.
75 Y. Zhu, S. An, X. Sun, D. Lan, J. Cui, Y. Zhang and W. He, *Chem. Eng. J.*, 2020, **383**, 123206.
76 J. Liu, J. Wang, B. Zhang, Y. Ruan, L. Lv, X. Ji, K. Xu, L. Miao and J. Jiang, *ACS Appl. Mater. Interfaces*, 2017, **9**, 15364–15372.
77 J. Fu, L. Li, J. M. Yun, D. Lee, B. K. Ryu and K. H. Kim, *Chem. Eng. J.*, 2019, **375**, 121939.
78 J.-Z. He, W.-J. Niu, Y.-P. Wang, Q.-Q. Sun, M.-J. Liu, K. Wang, W.-W. Liu, M.-C. Liu, F.-C. Yu and Y.-L. Chueh, *Electrochim. Acta*, 2020, **362**, 136968.
79 Z. Peng, C. Yang, Y. Hu, F. Bai, W. Chen, R. Liu, S. Jiang and H.-C. Chen, *Appl. Surf. Sci.*, 2022, **573**, 151561.
80 M. Zhang, H. Zheng, H. Zhu, M. Zhang, R. Liu, X. Zhu, X. Li and H. Cui, *J. Alloys Compd.*, 2022, **901**, 163633.
81 G. Shao, R. Yu, X. Zhang, X. Chen, F. He, X. Zhao, N. Chen, M. Ye and X. Y. Liu, *Adv. Funct. Mater.*, 2020, **30**, 2003153.
82 Y. Miao, X. Zhao, X. Wang, C. Ma, L. Cheng, G. Chen, H. Yue, L. Wang and D. Zhang, *Nano Res.*, 2020, **13**, 3041–3047.
83 A. Hu, J. Long, C. Shu, C. Xu, T. Yang, R. Liang and J. Li, *ChemElectroChem*, 2019, **6**, 349–358.
84 S. A. Ansari, S. Goumri-Said, H. M. Yadav, M. Belarbi, A. Aljaafari and M. B. Kanoun, *Sol. Energy Mater. Sol. Cells*, 2021, **225**, 111064.
85 H.-J. Kim and V. T.-V. Chebrolu, *New J. Chem.*, 2018, **42**, 18824–18836.
86 S. Vigneshwaran, C. M. Park and S. Meenakshi, *Sep. Purif. Technol.*, 2021, **258**, 118003.
87 J. Peng, J. Xu, Z. Wang, Z. Ding and S. Wang, *Phys. Chem. Chem. Phys.*, 2017, **19**, 25919–25926.
88 J. Yu, C. Lv, L. Zhao, L. Zhang, Z. Wang and Q. Liu, *Adv. Mater. Interfaces*, 2018, **5**, 1701396.
89 Z. Kang, H. Guo, J. Wu, X. Sun, Z. Zhang, Q. Liao, S. Zhang, H. Si, P. Wu, L. Wang and Y. Zhang, *Adv. Funct. Mater.*, 2019, **29**, 1807031.

90 P. K. Kannan, C. Hu, H. Morgan and C. S. Rout, *Chem.–Asian J.*, 2016, **11**, 1837–1841.
91 P. Hu, S. Dong, X. Li, J. Chen and P. Hu, *ACS Sustainable Chem. Eng.*, 2020, **8**, 10230–10241.
92 Y. Xu, X. Gao, W. Chu, Q. Li, T. Li, C. Liang and Z. Lin, *J. Mater. Chem. A*, 2016, **4**, 10248–10253.
93 Y. Xiao, J. Huang, Y. Xu, H. Zhu, K. Yuan and Y. Chen, *J. Mater. Chem. A*, 2018, **6**, 9161–9171.
94 L. Hou, R. Bao, M. Rehan, L. Tong, G. Pang, X. Zhang and C. Yuan, *Adv. Electron. Mater.*, 2017, **3**, 1600322.
95 P. Phonsuksawang, P. Khajondetchairit, T. Butburee, S. Sattayaporn, N. Chanlek, P. Hirunsit, S. Suthirakun and T. Siritanon, *Electrochim. Acta*, 2020, **340**, 135939.
96 P. Phonsuksawang, P. Khajondetchairit, K. Ngamchuea, T. Butburee, S. Sattayaporn, N. Chanlek, S. Suthirakun and T. Siritanon, *Electrochim. Acta*, 2021, **368**, 137634.
97 S. Abureden, F. M. Hassan, G. Lui, S. Sy, R. Batmaz, W. Ahn, A. Yu and Z. Chen, *J. Mater. Chem. A*, 2017, **5**, 7523–7532.
98 T. Peng, H. Yi, P. Sun, Y. Jing, R. Wang, H. Wang and X. Wang, *J. Mater. Chem. A*, 2016, **4**, 8888–8897.
99 M. Zhang, H. Liu, Z. Song, T. Ma and J. Xie, *Chem. Eng. J.*, 2020, **392**, 123669.
100 M. Liang, M. Zhao, H. Wang, J. Shen and X. Song, *J. Mater. Chem. A*, 2018, **6**, 2482–2493.
101 Y. Cui, J. Zhang, C. Jin, Y. Liu, W. Luo and W. Zheng, *Small*, 2018, **15**, e1804318.
102 X. Chen, D. Chen, X. Guo, R. Wang and H. Zhang, *ACS Appl. Mater. Interfaces*, 2017, **9**, 18774–18781.
103 L. Lin, J. Liu, T. Liu, J. Hao, K. Ji, R. Sun, W. Zeng and Z. Wang, *J. Mater. Chem. A*, 2015, **3**, 17652–17658.
104 C. Liu, X. Wu and B. Wang, *Chem. Eng. J.*, 2020, **392**, 123651.
105 M. L. Aparna, T. Thomas and G. R. Rao, *J. Electrochem. Soc.*, 2022, **169**, 020515.
106 L. Yang, X. Lu, S. Wang, J. Wang, X. Guan, X. Guan and G. Wang, *Nanoscale*, 2020, **12**, 1921–1938.
107 Y. Yan, A. Li, C. Lu, T. Zhai, S. Lu, W. Li and W. Zhou, *Chem. Eng. J.*, 2020, **396**, 125316.
108 X. Song, C. Huang, Y. Qin, H. Li and H. C. Chen, *J. Mater. Chem. A*, 2018, **6**, 16205–16212.
109 W. Chen, X. Zhang, L.-E. Mo, Y. Zhang, S. Chen, X. Zhang and L. Hu, *Chem. Eng. J.*, 2020, **388**, 124109.
110 X. Chen, C. He, W. Wang, T. Bai, G. Xue and M. Ye, *Phys. Rev. Appl.*, 2021, **15**, 064042.
111 W. He, C. Wang, H. Li, X. Deng, X. Xu and T. Zhai, *Adv. Energy Mater.*, 2017, **7**, 1700983.
112 Y. Sui, Y. Zhang, H. Hu, Q. Xu, F. Yang and Z. Li, *Adv. Mater. Interfaces*, 2018, **5**, 1800018.
113 C. Zhang, X. Cai, Y. Qian, H. Jiang, L. Zhou, B. Li, L. Lai, Z. Shen and W. Huang, *Adv. Sci.*, 2018, **5**, 1700375.
114 Z. Peng, L. Gong, J. Huang, Y. Wang, L. Tan and Y. Chen, *Carbon*, 2019, **153**, 531–538.
115 Q. Li, W. Lu, Z. Li, J. Ning, Y. Zhong and Y. Hu, *Chem. Eng. J.*, 2020, **380**, 122544.
116 J. Huang, J. Wei, Y. Xu, Y. Xiao and Y. Chen, *J. Mater. Chem. A*, 2017, **5**, 23349–23360.
117 T. Sun, C. Huang, H. Shu, L. Luo, Q. Liang, M. Chen, J. Su and X. Wang, *ACS Appl. Mater. Interfaces*, 2020, **12**, 57975–57986.
118 Y. Tang, X. Li, H. Lv, D. Xie, W. Wang, C. Zhi and H. Li, *Adv. Energy Mater.*, 2020, **10**, 2000892.
119 J. Zhang, K. Song, L. Mi, C. Liu, X. Feng, J. Zhang, W. Chen and C. Shen, *J. Phys. Chem. Lett.*, 2020, **11**, 1435–1442.
120 S. Li, P. Ge, F. Jiang, H. Shuai, W. Xu, Y. Jiang, Y. Zhang, J. Hu, H. Hou and X. Ji, *Energy Storage Materials*, 2019, **16**, 267–280.
121 Y. V. Lim, S. Huang, J. Hu, D. Kong, Y. Wang, T. Xu, L. K. Ang and H. Y. Yang, *Small Methods*, 2019, **3**, 1900112.
122 Z. Xiong, L. Huang, J. Peng, Y. Hou, Z. Ding and S. Wang, *ChemCatChem*, 2019, **11**, 5513–5518.
123 B. He, J.-J. Song, X.-Y. Li, C.-Y. Xu, Y.-B. Li, Y.-W. Tang, Q.-L. Hao, H.-K. Liu and Z. Su, *Nanoscale*, 2021, **13**, 810–818.
124 F. Wang, G. Li, X. Meng, S. Xu and W. Ma, *J. Power Sources*, 2020, **462**, 228162.
125 W. Liu, J. Zhang, Z. Bai, G. Jiang, M. Li, K. Feng, L. Yang, Y. Ding, T. Yu, Z. Chen and A. Yu, *Adv. Funct. Mater.*, 2018, **28**, 1706675.
126 X. Zuo, Y. Song and M. Zhen, *Appl. Surf. Sci.*, 2020, **500**, 144000.
127 F. Yang, Y. Shen, Z. Cen, J. Wan, S. Li, G. He, J. Hu and K. Xu, *Sci. China Mater.*, 2021, **65**, 356–363.
128 S. Li, P. Xu, M. K. Aslam, C. Chen, A. Rashid, G. Wang, L. Zhang and B. Mao, *Energy Storage Materials*, 2020, **27**, 51–60.
129 J. Zhang, X. Bai, T. Wang, W. Xiao, P. Xi, J. Wang, D. Gao and J. Wang, *Nano-Micro Lett.*, 2019, **11**, 2.
130 S. Hyun, B. Son, H. Kim, J. Sanetuntikul and S. Shanmugam, *Appl. Catal., B*, 2020, **263**, 118283.
131 X. Zhao, H. Liu, Y. Rao, X. Li, J. Wang, G. Xia and M. Wu, *ACS Sustainable Chem. Eng.*, 2019, **7**, 2610–2618.
132 X. Du, X. Zhang, Y. Li and M. Zhao, *Int. J. Hydrogen Energy*, 2018, **43**, 19955–19964.
133 X. Feng, Q. Jiao, H. Cui, M. Yin, Q. Li, Y. Zhao, H. Li, W. Zhou and C. Feng, *ACS Appl. Mater. Interfaces*, 2018, **10**, 29521–29531.
134 Y. Gong, Y. Lin, Z. Yang, J. Wang, H. Pan, Z. Xu and Y. Liu, *ChemistrySelect*, 2019, **4**, 1180–1187.
135 F. Li, R. Xu, Y. Li, F. Liang, D. Zhang, W.-F. Fu and X.-J. Lv, *Carbon*, 2019, **145**, 521–528.
136 H. Li, L. Chen, P. Jin, Y. Li, J. Pang, J. Hou, S. Peng, G. Wang and Y. Shi, *Nano Res.*, 2021, **15**, 950–958.
137 J. Zhou, Y. Dou, T. He, A. Zhou, X.-J. Kong, X.-Q. Wu, T. Liu and J.-R. Li, *Nano Res.*, 2021, **14**, 4548–4555.
138 L. Sha, K. Ye, G. Wang, J. Shao, K. Zhu, K. Cheng, J. Yan, G. Wang and D. Cao, *Chem. Eng. J.*, 2019, **359**, 1652–1658.
139 D. Khalafallah, Q. Zou, M. Zhi and Z. Hong, *Electrochim. Acta*, 2020, **350**, 136399.
140 B. Li, C. Song, J. Rong, J. Zhao, H.-E. Wang, P. Yang, K. Ye, K. Cheng, K. Zhu, J. Yan, D. Cao and G. Wang, *J. Energy Chem.*, 2020, **50**, 195–205.
141 X. Du, W. Lian and X. Zhang, *Int. J. Hydrogen Energy*, 2018, **43**, 20627–20635.

142 X.-X. Li, X.-T. Wang, K. Xiao, T. Ouyang, N. Li and Z.-Q. Liu, *J. Power Sources*, 2018, **402**, 116–123.
143 S. S. Rao, I. K. Durga, N. Kundakarla, D. Punnoose, C. V. V. M. Gopi, A. E. Reddy, M. Jagadeesh and H.-J. Kim, *New J. Chem.*, 2017, **41**, 10037–10047.
144 L. Li, X. Zhang, S. a. Liu, B. Liang, Y. Zhang and W. Zhang, *Sol. Energy*, 2020, **202**, 358–364.
145 K. S. Anuratha, S. Mohan and S. K. Panda, *New J. Chem.*, 2015, **40**, 1785–1791.
146 J. Qiu, D. He, H. Wang, W. Li, B. Sun, Y. Ma, X. Lu and C. Wang, *Electrochim. Acta*, 2021, **367**, 137451.
147 P. Su, Q. Jiao, H. Li, Y. Li, X. Liu, Q. Wu, D. Shi, Y. Zhao, T. Wang and W. Wang, *ACS Appl. Energy Mater.*, 2021, **4**, 4344–4354.
148 L. Nie and Q. Zhang, *Inorg. Chem. Front.*, 2017, **4**, 1953–1962.
149 X.-Q. Qiao, Z.-W. Zhang, Q.-H. Li, D. Hou, Q. Zhang, J. Zhang, D.-S. Li, P. Feng and X. Bu, *J. Mater. Chem. A*, 2018, **6**, 22580–22589.
150 X.-Q. Qiao, Z.-W. Zhang, F.-Y. Tian, D.-F. Hou, Z.-F. Tian, D.-S. Li and Q. Zhang, *Cryst. Growth Des.*, 2017, **17**, 3538–3547.
151 S. Zhao, J. Xu, M. Mao, L. Li and X. Li, *Appl. Surf. Sci.*, 2020, **528**, 147016.
152 K. Jiang, W. Iqbal, B. Yang, M. Rauf, I. Ali, X. Lu and Y. Mao, *J. Alloys Compd.*, 2021, **853**, 157284.
153 K. J. Babu, T. R. Kumar, D. J. Yoo, S.-M. Phang and G. G. Kumar, *ACS Sustainable Chem. Eng.*, 2018, **6**, 16982–16989.
154 Q. Guo, T. Wu, L. Liu, Y. He, D. Liu and T. You, *J. Alloys Compd.*, 2020, **819**, 153376.
155 D. Chen, H. Wang and M. Yang, *Anal. Methods*, 2017, **9**, 4718–4725.
156 D. Li, X. Zhang, L. Pei, C. Dong, J. Shi and Y. Xu, *Inorg. Chem. Commun.*, 2019, **110**, 107581.
157 Y. He, T. Wu, J. Wang, J. Ye, C. Xu, F. Li and Q. Guo, *Talanta*, 2020, **219**, 121277.
158 B. Li, J. Xia, J. Liu, Q. Liu, G. Huang, H. Zhang, X. Jing, R. Li and J. Wang, *Chem. Phys. Lett.*, 2018, **703**, 80–85.
159 M. Zhou, W. Gu, G. Wang, J. Zheng, C. Pei, F. Fan and G. Ji, *J. Mater. Chem. A*, 2020, **8**, 24267–24283.
160 M. Green and X. Chen, *J. Materiomics*, 2019, **5**, 503–541.
161 R. Peymanfar and S. Ghorbanian-Gezaforodi, *Nanotechnology*, 2020, **31**, 495202.
162 J. Liu, Z. Yang, L. Yang, Y. Zhu, T. Xue and G. Xu, *J. Alloys Compd.*, 2021, **853**, 157403.
163 S. Dong, P. Hu, X. Li, C. Hong, X. Zhang and J. Han, *Chem. Eng. J.*, 2020, **398**, 125588.
164 P. Hu, S. Dong, F. Yuan, X. Li and C. Hong, *Adv. Compos. Hybrid Mater.*, 2021, DOI: 10.1007/s42114-021-00318-w.
165 Z. Sun, C. Zhao, X. Cao, K. Zeng, Z. Ma, Y. Hu, J.-H. Tian and R. Yang, *Electrochim. Acta*, 2020, **338**, 135900.
166 L. Xing, X. Zheng, M. Schroeder, J. Alvarado, A. von Wald Cresce, K. Xu, Q. Li and W. Li, *Acc. Chem. Res.*, 2018, **51**, 282–289.